(4)

College of Earth and Mineral Sciences

PENNSTATE

ANNUAL TECHNICAL REPORT

December 1989

OFFICE OF NAVAL RESEARCH

Contract NO. N0014-86-K-0133

HIGH TEMPERATURE OXIDATION AND ELECTROCHEMICAL STUDIES RELATED TO HOT CORROSION

D-H. Kim, R. Reidy, and G. Simkovich

Department of Materials Science and Engineering
The Pennsylvania State University
University Park, Pennsylvania 16802

PENN STATE
College of Earth and Mineral Sciences

Undergraduate Majors

Ceramic Science and Engineering, Fuel Science, Metals Science and Engineering, Polymer Science; Mineral Economics; Mining Engineering, Petroleum and Natural Gas Engineering; Earth Sciences, Geosciences; Geography; Meteorology.

Graduate Programs and Fields of Research

Ceramic Science and Engineering, Fuel Science, Metals Science and Engineering, Polymer Science; Mineral Economics; Mining Engineering, Mineral Processing, Petroleum and Natural Gas Engineering;
Geochemistry and Mineralogy, Geology, Geophysics; Geography; Meteorology.

Universitywide Interdisciplinary Graduate Programs Involving EMS Faculty and Students

Earth Sciences, Ecology, Environmental Pollution Control Engineering, Mineral Engineering Management, Solid State Science.

Associate Degree Programs

Metallurgical Engineering Technology (Shenango Valley Campus).

Interdisciplinary Research Groups Centered in the College

C. Drew Stahl Center for Advanced Oil Recovery, Center for Advanced Materials, Coal Research Section, Earth System Science Center, Mining and Mineral Resources Research Institute, Ore Deposits Research Group.

Analytical and Characterization Laboratories (Mineral Constitution Laboratories)

Services available include: classical chemical analysis of metals and silicate and carbonate rocks; X-ray diffraction and fluorescence; electron microscopy and diffraction; electron microprobe analysis; atomic absorption analysis; spectrochemical analysis; surface analysis by secondary ion mass spectrometry (SIMS); and scanning electron microscopy (SEM).

U.Ed. 87-1027
Produced by the Penn State Department of Publications

SECURITY CLASSIFICATION OF THIS PAGE

REPORT DOCUMENTATION PAGE

1a. REPORT SECURITY CLASSIFICATION	1b. RESTRICTIVE MARKINGS
2a. SECURITY CLASSIFICATION AUTHORITY	3. DISTRIBUTION/AVAILABILITY OF REPORT
2b. DECLASSIFICATION/DOWNGRADING SCHEDULE	
4. PERFORMING ORGANIZATION REPORT NUMBER(S) Metallurgy Program, 209 Steidle Bldg.	5. MONITORING ORGANIZATION REPORT NUMBER(S)
6a. NAME OF PERFORMING ORGANIZATION Metallurgy Program 6b. OFFICE SYMBOL (If applicable)	7a. NAME OF MONITORING ORGANIZATION Metallurgy Branch
6c. ADDRESS (City, State and ZIP Code) 209 Steidle Bldg. The Pennsylvania State University University Park, PA 16802	7b. ADDRESS (City, State and ZIP Code) Office of Naval Research Arlington, VA 22217
8a. NAME OF FUNDING/SPONSORING ORGANIZATION Metallurgy Branch 8b. OFFICE SYMBOL (If applicable)	9. PROCUREMENT INSTRUMENT IDENTIFICATION NUMBER N0014-86-K-0133 (contract number)
8c. ADDRESS (City, State and ZIP Code) Office of Naval Research Arlington, VA 22217	10. SOURCE OF FUNDING NOS. PROGRAM ELEMENT NO. / PROJECT NO. / TASK NO. / WORK UNIT NO.
11. TITLE (Include Security Classification) High Temperature Oxidation and Electrochemical Studies Related to Hot Corrosion	
12. PERSONAL AUTHOR(S) D-H. Kim, R. Reidy, and G. Simkovich	
13a. TYPE OF REPORT Annual Technical Report 13b. TIME COVERED FROM 1-89 TO 1-90	14. DATE OF REPORT (Yr., Mo., Day) 90-15-2 15. PAGE COUNT
16. SUPPLEMENTARY NOTATION	

17. COSATI CODES			18. SUBJECT TERMS (Continue on reverse if necessary and identify by block number)
FIELD	GROUP	SUB. GR.	

19. ABSTRACT (Continue on reverse if necessary and identify by block number)

In order to aid in further understanding hot corrosion processes, investigations of the electrical behavior of molten Na_2SO_4 have been undertaken. Wagner Hebb type polarization experiments and total electrical conductivity measurements by an A.C. impedance technique were carried out on melts of Na_2SO_4, both pure and those containing 10^{-3} m/o, 10^{-2} m/o, 10^{-1} m/o, and supersaturated (1m/o) Cr_2O_3, as a function of Na_2O activity at 1173 K.

It was observed that the total electrical conductivity ofpure Na_2SO_4 was of the order of 2.33×10^{-1} $(ohm\text{-}cm)^{-1}$ and varied only slightly with changes in the activity of Na_2O. From the Wagner-Hebb type D.C. polarization experiments on pure Na_2SO_4, the electron conductivity was shown to be much greater than the electron hole conductivity over the entire ranges of Na_2O activities. The partial conductivity of electrons in Na_2SO_4 was about two orders of magnitude less than the total electrical conductivity. Thus the transport number of electrons, t_e, is of the order of 10^{-3} in a pure Na_2SO_4 melt at 1173 K.
(see back)

20. DISTRIBUTION/AVAILABILITY OF ABSTRACT UNCLASSIFIED/UNLIMITED ☐ SAME AS RPT. ☐ OTIC USERS ☐	21. ABSTRACT SECURITY CLASSIFICATION
22a. NAME OF RESPONSIBLE INDIVIDUAL	22b. TELEPHONE NUMBER (Include Area Code) 22c. OFFICE SYMBOL

DD FORM 1473, 83 APR EDITION OF 1 JAN 73 IS OBSOLETE.

SECURITY CLASSIFICATION OF THIS PAGE

From the potentiostatic polarization technique, the cation transport number of a pure sodium sulfate melt was found to be about 0.98 at 1173 K.

The introduction of Cr_2O_3 in Na_2SO_4 at 1173 K decreases the total electrical conductivities as a function of chromium oxide concentration in the melts. The addition of Cr_2O_3 in the melt increases the electron hole conductivities and decreases the electron conductivities as compared to that of a pure Na_2SO_4 melt at 1173 K.

Additionally, studies were conducted to examine the nature of vanadium hot corrosion on two ceramic coatings (alumina and zirconia). Experiments showed significant solubility V_2O_5 in Al_2O_3 while apparently causing little surface corrosion of the alumina. Similar work with stabilized zirconia samples evidenced definite corrosive dissolution of the surface. Electrical conductivities of a variety of partially-densified stabilized zirconia samples were measuredto determine the effect of porosity on electrical transport. Thermodynamic models of both the Al_2O_3-Na_2SO_4-V_2O_5 and the stabilized zirconia-Na_2SO_4-V_2O_5 systems were described and compared to experimental data.

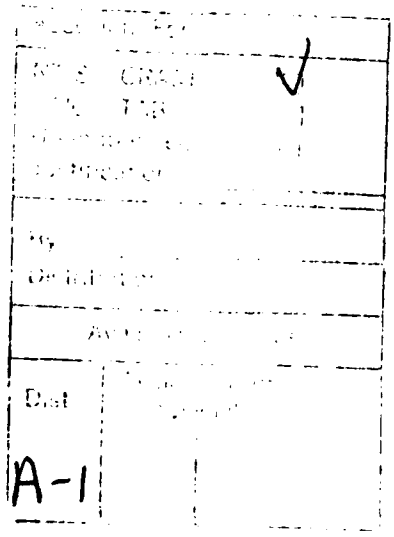

ABSTRACT

In order to aid in further understanding hot corrosion processes, investigations of the electrical behavior of molten Na_2SO_4 have been undertaken. Wagner-Hebb type polarization experiments and total electrical conductivity measurements by an A.C. impedance technique were carried out on melts of Na_2SO_4, both pure and those containing 10^{-3} m/o, 10^{-2} m/o, 10^{-1} m/o and supersaturated (1 m/o) Cr_2O_3, as a function of Na_2O activity at 1173 K.

It was observed that the total electrical conductivity of pure Na_2SO_4 was of the order of 2.33×10^{-1} $(ohm\text{-}cm)^{-1}$ and varied only slightly with changes in the activity of Na_2O. From the Wagner-Hebb type D.C. polarization experiments on pure Na_2SO_4, the electron conductivity was shown to be much greater than the electron hole conductivity over the entire range of Na_2O activities. The partial conductivity of electrons in Na_2SO_4 was about two orders of magnitude less than the total electrical conductivity. Thus, the transport number of electrons, t_θ, is of the order of 10^{-3} in a pure Na_2SO_4 melt at 1173 K. From the potentiostatic polarization technique, the cation transport number of a pure sodium sulfate melt was found to be about 0.98 at 1173 K.

The introduction of Cr_2O_3 into Na_2SO_4 melts at 1173 K decreases the total electrical conductivities as a function of chromium oxide concentration in the melts. The addition of Cr_2O_3 in the melt increases the electron hole conductivities and decreases the electron conductivities as compared to that of a pure Na_2SO_4 melt at 1173 K.

Additionally, studies were conducted to examine the nature of vanadium hot corrosion on two ceramic coatings (alumina and zirconia). Experiments showed significant solubility of V_2O_5 in Al_2O_3 while apparently causing little surface corrosion of the alumina. Similar work with stabilized zirconia samples evidenced definite corrosive dissolution of the surface. Electrical conductivities of a variety of partially-densified

stabilized zirconia samples were measured to determine the effect of porosity on electrical transport. Thermodynamic models of both the Al_2O_3 -Na_2SO_4-V_2O_5 and the stabilized zirconia-Na_2SO_4-V_2O_5 systems were described and compared to experimental data.

I. INTRODUCTION

Hot corrosion is generally defined in broad terms as an accelerated or catastrophic oxidation of alloys and other materials. This form of attack is particularly severe in the temperature range of 1033 - 1273 K, and it has affected both aircraft engines and industrial gas turbines. There is a general agreement that condensed alkali metal salts, notably Na_2SO_4, are a prerequisite to hot corrosion. The source of this salt may be (a) the direct ingestion of sea salt in a marine environment, (b) the formation of Na_2SO_4 during combustion of fuels containing both sodium and sulfur, (c) the formation of Na_2SO_4, during combustion, from sodium - contaminated, airborne dust and sulfur in the fuel [1].

The exact mechanisms of hot corrosion are still uncertain, but from many studies on the hot corrosion mechanisms of metals and alloys, the various mechanisms that have been proposed can be broadly classified into two categories : (a) acidic - basic fluxing models [2-4] and (b) dissolution - reprecipitation electrochemical model [5]. The overall mechanisms of hot corrosion involve the dissolution of normally protective oxide layers and the formation of porous, nonadherent, and hence unprotective scales when alloy surfaces are covered by a thin film of liquid sodium sulfate. It appears that the initial formation of metal oxides is necessary for the initial reaction and the transport of oxygen through the molten salt phase is required to form such metal oxides.

Little is known about the electronic transport properties in molten Na_2SO_4. This study is, therefore, concerned with obtaining such information to aid in the elucidation of the mechanism of the process. A potentiostatic polarization technique was employed to estimate the ionic transport numbers of a pure sodium sulfate melt at 1173 K. The electronic conductivities by Wagner-Hebb type polarization studies [6,7] as well as total electrical conductivity measurements by an A.C. impedance technique were carried out on molten Na_2SO_4 as a function of Na_2O activities at 1173 K since the proposed models

which describe the degradation behavior of alloys are strongly dependent on SO_2, O_2, and /or SO_3 gas pressure, i.e., the Na_2O activity in the Na_2SO_4 deposit. The transport numbers of electronic species in Na_2SO_4 melt were evaluated by dividing the values of electronic conductivities by those of total electrical conductivities. Additionally, such studies were conducted in molten Na_2SO_4 containing Cr_2O_3 to elucidate the effect of Cr_2O_3 on the transport mechanism in the Na_2SO_4 melt at 1173 K.

Another form of hot corrosion is vanadium attack. Vanadium enters the turbine as a fuel impurity in organic and inorganic forms. These compounds react with oxygen to form oxides (VO, VO_2, VO_3, and V_2O_5) and hydroxides ($V_2O_7H_4$, $VO(OH)_3$, and $VO_2(OH)_2$).[8] These gases either condense onto the turbine blades and react with sodium compounds to form sodium vanadates as in equations 1.1-1.3),

$$2VO(OH)_3(g) = V_2O_5(l) + 3H_2O(g) \qquad 1.1)$$

$$V_2O_5(g) = V_2O_5(l) \qquad 1.2)$$

$$V_2O_5(l) + Na_2O(l) = 2NaVO_3(l) \qquad 1.3)$$

or react with sodium compounds in the gas phase forming sodium vanadates which condense onto the turbine blades as in equation 1.4).

$$VO(OH)_3(g) + NaOH(g) = NaVO_3(l) + 2H_2O(g) \qquad 1.4)$$

In addition to Na_2SO_4, Luthra and Spacil found both V_2O_5 and $NaVO_3$ in the condensate; therefore it is difficult to determine which compound is more destructive to the oxide.[8] Further, one can not ignore the effects of Na_2SO_4 in a separate or combined attack on the oxide scale.

In vanadium attack, a similar dissolution mechanism utilizes the Lewis definition of acids (electron acceptors) and bases (electron donors). Jones describes the ability of vanadium pentoxide to behave as a Lewis acid and react with a protective oxide.[9]

$$Y_2O_3\ (s) + V_2O_5(l) = 2YVO_4(l) \qquad 1.5)$$

(base) (acid) (salt)

This dissolution mechanism involves the transport of electrons from the stabilizing component to the corrosive V_2O_5. A greater understanding of this transport phenomenon could yield the ability to retard or halt this dissolution.

The type and concentration of point defects in an oxide is often dependent on the temperature, pressure, and chemical potentials of the oxide components.[10] Atomic defects (vacancies, interstitials, impurities, or misplaced atoms) affect solid state diffusion and non-stoichiometry of compounds. Changes in these properties, in turn, alter reaction rates, ionic conductivities, and sintering rates. Electronic defects (electrons and electron holes) determine electrical conductivities and thermoelectric power as well as other properties.[10,11] Therefore, a detailed understanding of the point defect behavior of a compound would provide great insight or even allow one to predict the transport phenomena in that material. Additionally, one may alter the transport properties of a compound by changing the nature or concentration of the point defects within it.

In recent years, efforts have been made to apply protective ceramic coatings to turbine blades to improve resistance to hot corrosion as well as to increase engine operating temperatures.[12-14] These materials are referred to as thermal barrier coatings. With additions of various stabilizers, zirconia has been used as a thermal barrier coating.

Pure zirconium oxide is a polymorphic compound. Three different stable forms of zirconia exist: cubic (fluorite structure, 2370 - 2680°C), tetragonal (1170 - 2370°C), and

monoclinic (below 1170°C).[15] The phase transition from tetragonal to monoclinic has caused considerable concern. Early studies have determined that the transformation is martensitic [16] and does not occur at a fixed temperature, but over a temperature range, and involves a large (about 9%) volume expansion. This volume increase causes cracking in the ZrO_2 when cooled below the transition; therefore traditional cooling methods to below 1170°C can result in crumbling of the zirconia.

The addition of CaO, MgO, Y_2O_3, and CeO_2 to zirconia lowers the transition temperatures of both solid state phase transformations.[15] Stubican and Hellmann [17] have reviewed the binary oxide phase diagrams and have shown a partially stabilized form (a mixture of cubic and tetragonal or monoclinic phases) and a fully stabilized zirconia (cubic phase). Both the cubic and mixed phases are stable at room temperature.

An important thrust of this work is to determine the effect of point defects on the mechanisms and transport properties involved in the hot corrosion of zirconia coatings. It is prudent to briefly review the recent efforts to study these mechanisms by other methods.[8,18,19] The sulfidation and vanadium attack studies by Jones and Williams [20,21] demonstrated that ZrO_2 is substantially more resistant to hot corrosion than the dopants, Y_2O_3, CeO_2, and HfO_2. In other work, Jones discusses the degradation of the coating with respect to the acid-base reaction model.[9] The V_2O_5 reacts with the Y_2O_3 in the zirconia and forms a yttrium vanadate (equation 1.5)). The removal of yttria destabilizes the zirconia allowing the more voluminous monoclinic phase to form and leading to surface cracking of the coating. As the protective scale is thermally cycled, the cracks propagate and extend into the coating causing spallation. This mechanism has been put forth by a number of other investigators.[22-24]

II. THEORETICAL BACKGROUND

(i) Total Conductivity Measurement

A.C. impedance measurements were conducted to obtain polarization free total electrical conductivity of molten sodium sulfate and the melts containing Cr_2O_3. In D.C. techniques, a space charge of either ions or electrons form in the vicinity of the electrodeswhich leads to a non-uniform field across the specimen. However, in A.C. impedance techniques, the use of small amplitude sinusoidal potentials does not disturb the electrode properties and at higher frequencies polarization of the specimen electrode may be eliminated. Thus, an A.C. impedance technique was utilized to measure the resistance of a pure Na_2SO_4 melt and melts containing Cr_2O_3 since the melts showed some polarization effects at the electrodes in our preliminary D.C. experiments.

Impedance can be thought of as the resistance of a circuit to an alternating waveform as opposed to a pure resistance; it has not only magnitude but also direction - phase angle. One of the advantages of A.C. impedance techniques over conventional D.C. electrical conductivity efforts is the ability to separate the real and imaginary components of impedance. An impedance, Z, can be completely defined by specifying the magnitude, |Z|, and the angle, ø, or alternatively by specifying the magnitude of its real , Z', and imaginary, Z", components [25].

There are a number of graphical interpretations available for impedance data analysis over a wide frequency range [26]. A plot of Z' versus wZ" was employed to evaluate the resistance of the molten salts. A plot of Z' versus wZ" shows a straight line with a slope of $-R_pC$ and an intercept of $R_\Omega + R_p$ according to the following equation:

$$Z' = R_\Omega + R_p - R_p C w Z'' \qquad (2.1)$$

where Z' is the real part of the impedance

Z" is the imaginary part of the impedance

R_Ω is the resistance of the electrolyte

R_p is the polarization resistance

C is the capacitance

w is angular frequency ($= 2\pi f$)

The real and imaginary part of the impedance can be expressed by the following relationship [27].

$$Z' = R_\Omega + \frac{R_p}{1 + w^2C^2R_p^2} \qquad (2.2)$$

$$Z'' = \frac{wCR_p^2}{1 + w^2C^2R_p^2} \qquad (2.3)$$

Thus, as frequency increases, the straight line of a plot of Z' versus wZ" levels off,and the projection of this point onto the Z' axis affords the sum of the resistances of the electrolyte and the circuit leads according to the equation (2.2).

(ii) Electronic Conductivity Measurement

The idea that an appropriate choice of electrodes enables the suppression of either ionic or electronic transport in a galvanic cell provides the basis for the polarization technique. This technique has been extensively employed to investigate electronic conductivity in ionic solids [28-33] and has also been applied to a few molten systems [34-36].

Wagner [6] has derived the appropriate relation for the polarization conditions from transport theory. This relation states that, under steady state conditions, the total current due to passage of electronic species through the polarization cell is given by

$$I_{elect} = I_{\theta} + I_{\oplus}$$

$$= \frac{RTA}{LF}\left\{ \sigma^{o}_{\theta}\left[1-\exp\left(-\frac{EF}{RT}\right)\right] + \sigma^{o}_{\oplus}\left[\exp\left(\frac{EF}{RT}\right) - 1\right]\right\} \qquad (2.4)$$

where $I_{\theta}, I_{\oplus}$: electron and electron hole currents, respectively

$\sigma_{\theta}^{\circ}, \sigma_{\oplus}^{\circ}$: electron and electron hole conductivity, respectively

E : applied voltage

F : Faraday constant

R : gas constant

T : temperature (K)

L/A : cell constant.

In the derivation of equation (2.4) it is assumed [35,36] that

(i) excess electrons and holes follow the laws of ideal dilute solutions,

(ii) their mobilities are independent of concentrations,

(iii) the change in the concentration of atomic defects arising from thermal disorder with variation in the metal to nonmetal ratio is small,

(iv) convection in the melt is negligible.

The division of equation (2.4) by [1-exp(-EF/RT)] and rearrangement gives

$$I_{elect}\left\{\frac{LF}{RTA}\left[\frac{1}{1-\exp\left(-\frac{EF}{RT}\right)}\right]\right\} = \sigma_{\theta}^{\circ} + \sigma_{\oplus}^{\circ}\exp\left(\frac{EF}{RT}\right) \qquad (2.5)$$

and a plot of the left hand side of equation (2.5) versus exp (EF/RT) gives $\sigma\theta^{\circ}$ as the intercept and $\sigma\oplus^{\circ}$ as the slope. These values, combined with total electrical conductivity results, permit the evaluation of the transport numbers of each electronic carrier in the molten salts.

In the present work, D.C. current flowing through the polarization cell is measured at various applied voltages which are kept below the decomposition potentials of the sample to ensure that the measured current is only the electronic current.

(iii) Evaluation of Ionic Transport Numbers

The potentiostatic polarization cell technique was employed to determine ionic transport numbers for molten sodium sulfate at 1173 K. In a recent application of this technique, reasonable agreement was obtained with transport numbers from Tubandt and tracer diffusion techniques [37]. This technique is based on a two electrode cell. A constant D.C. potential is applied by a potentiostat and the current is monitored as a function of time. The electrode is chosen to be reversible with respect to the cation present in the electrolyte.

Under the influence of a D.C. field cations migrate to the negative electrode and anions to the positive electrode. As the concentration of anions increases near the positive electrode, local charge neutrality requires that a cation accompany each anion. This process establishes a salt concentration gradient across the electrolyte. As the cell polarizes the amount of current carried by the anion decreases but the amount carried by the cation remains constant. When the back potential created by the concentration gradient exactly

opposes the applied potential, the anions no longer carry current, and the cell is completely polarized with respect to the anion. Thus, the ratio of final current due to the cation only to the initial current due to the cation and anion yields the cation transport numbers of molten Na_2SO_4.

III. EXPERIMENTAL PROGRAM

(i) Gas Control

Variations on our previous measurements [38] were performed. In particular instead of using the SO_2/O_2 obtained by flowing helium over a $ZnO/ZnSO_4$ mixture, mass flow control meters (MKS Model 1259B) coupled with 4 channel readout (MKS Type 247C) were utilized for better control of SO_2/O_2 ratios.

(ii) A.C. Impedance Measurements

A.C. impedance measurements were performed to obtain polarization free total electrical conductivity. As shown in Figure 1, the three electrode system was utilized for the A.C. impedance measurements. The reference electrode was a silver wire immersed into a 10 m/o Ag_2SO_4/Na_2SO_4 melt contained in the Na ion conducting membrane, a mullite tube (0.7 cm O.D.) [39]. Pure gold wires serve as the working electrode and counter electrode. Platinum wires welded to these electrodes were employed as leads to connect to the EG & G Model 273 potentiostat coupled with Model 5208 Lock-In amplifier. The schematic arrangements for the A.C. impedance measurements are depicted in Figure 2.

The total electrical conductivity of a pure Na_2SO_4 melt and the melts containing various oxides was determined by measuring the resistance of the melts from the relation:

$$R = \left(\frac{1}{\sigma} \right) \text{Cell Constant} \qquad (3.1)$$

where R is the resistance measured in ohms, σ is the conductivity of the melt expressed in $(\text{ohm-cm})^{-1}$ and the cell constant is given in terms of cm^{-1}.

The cell constant, which is a characteristic of the conductivity cell, depends on the length between the electrodes and the surface area of the electrode exposed to the melt. The cell constant is usually predetermined by measuring the resistance across an ionic solution of known specific conductivity. Since the specific conductivity values of KCl solution are well established [23], an 0.1 N KCl solution was employed to determine the cell constant for the proposed work. The cell constant measurements were conducted at about 25°C utilizing identical cell arrangements with the gold crucible to contain an 0.1 N potassium chloride solution instead of the melt.

(iii) Wagner - Hebb Type Polarization Experiments

The Wagner-Hebb type polarization technique was used to determine the partial electronic conductivities of a pure Na_2SO_4 melt and melts containing Cr_2O_3 as a function of Na_2O activity at 1173 K. A constant voltage was supplied to the polarization cell via the EG & G Model 273 potentiostat. A Solid State Electrometer, Model 610C was utilized to check the actual voltage on the polarization cell. The reference electrode was the same as that used in A.C. impedance experiments. Platinum wires were employed to lead two gold electrodes into the potentiostat. Pure gold crucibles were used for these experiments. An A.C. impedance technique was utilized to determine the cell constant with the same cell

geometry by measuring the conductivity of an 0.1 N KCl solution instead of the molten salts.

(iv) Potentiostatic Polarization Experiment

Most molten salts are ionic conductors. Thus, it seems logical to assume that molten sodium sulfate is an ionic conductor. The relative contributions of the different carrier species (cation vs. anion) was investigated by this technique. A constant D.C. potential was applied via the potentiostat and the current was monitored automatically as a function of time. A symmetric cell configuration was employed, and the electrode was chosen to match the cation in the molten sodium sulfate. The reversible electrode consists of a mullite tube conductive to sodium ions containing a silver electrode immersed into a melt of Ag_2SO_4- 90 m/o Na_2SO_4. Mullite is a two-phase ceramic consisting of mullite grains ($3Al_2O_3$ - $2SiO_2$) enveloped by silica. At high temperatures, dissolved alkali metal compounds in the silica film allow transport of alkali metal cations under an electrochemical driving force with essentially no electronic conduction [41,42].

(v) Vanadium and Zirconia Experiments

(a) Thermodynamic Modelling

To predict the stabilities of the reaction products of vanadic attack, thermodynamic modelling using SOLGASMIX has been used . This computer program allows one to vary the reaction temperatures, mole fractions of the reactants, and the chemicals activities. Although large deviations from ideality and kinetic contributions can reduce the reliability of this thermodynamic model, predicted reactions can shed light on experimental results.

(b) Sample Preparation

Alumina samples were cut from 99.8% (5mm dia.) Al_2O_3 rods using an Isomet low speed saw. Zirconia samples were prepared from a variety of powders. The powders were pressed uniaxially in a 6 mm die at 5000 psi, cold isostatically pressed to 20 kpsi, and sintered in air at 1500-1650 C for 1-5 hours.

(c) Qualitative Investigation of Vanadium Corrosion

To better understand the solubility behavior and surface corrosion caused by vanadium compounds, samples were subjected to vanadic attack. The alumina samples were exposed to large and small quantities (.1-2 weight% of the sample) of V_2O_5 in air at 900 and 1000 C. Similar experiments were conducted on the zirconia samples at 700 and 900 C. The exposed materials were then examined using optical and electron microscopy.

(d) AC Conductivity Measurements

Electrical conductivity measurements were used to examine the electrical transport in zirconia as well as to serve as a data base for later experiments. These future experiments (AC impedance and DC polarization) with the addition of conductivity data will provide valuable insight to the transport mechanisms in zirconia and, consequently, vanadium hot corrosion. The samples were placed between two platinum electrodes, and their conductivities were measured using an AC digital bridge.

IV. RESULTS and DISCUSSION

(i) Pure Na_2SO_4

The measured total electrical conductivities of a pure Na_2SO_4 at 1173 K are depicted in Figure 3 as a function of the activity of Na_2O in the melt. The total electrical conductivities remain rather constant regardless of the changes in Na_2O activities. The total electrical conductivity of a pure Na_2SO_4 melt averaged about 0.233 $(ohm\text{-}cm)^{-1}$ which is about one order of magnitude less than the literature values [43-46]. This discrepancy is most probably caused by the facts that the previous investigators had: (1) a relatively impure Na_2SO_4, (2) a reaction between their quartz capillary and molten sodium sulfate, and (3) a reaction with their Pt electrodes. It was observed that there was significant deterioration of the quartz crucibles used to contain the Na_2SO_4 melts in our preliminary work, and that there was a reaction of Na_2SO_4 melts with Pt electrodes initially utilized.

From the Wagner-Hebb type polarization measurements on pure Na_2SO_4 melt at 1173 K, the partial conductivities of electrons and electron holes were obtained and are depicted in Figure 4. It can be seen that electron conduction in pure Na_2SO_4 is considerably larger than that of electron holes over the entire Na_2O activity range. Furthermore, it is noted that both electron and electron hole conductivities remain relatively constant regardless of the changes in Na_2O activities. Thus, the total electrical conductivity as well as partial electronic conductivities of a pure Na_2SO_4 melt are not dependent on the acidity and/or basicity of the melt.

From the measured values of total electrical conductivities and electronic conductivities, the transport numbers of electronic species may be computed. These numbers are plotted in Figure 5 for a pure Na_2SO_4 melt. The transport numbers of electrons are of the order of 10^{-3} while those of electron holes are of the order of 10^{-4}.

This indicates that the electronic conduction in a pure Na_2SO_4 melt arises primarily via electron transport over the whole Na_2O activity range. The transport numbers of electronic species in molten salts have not been measured extensively but the few that have been measured are similar to those determined in this study, e.g., $t_\theta = 3x10^{-3}$ in the molten eutectic of LiCl-KCl at 450°C [47].

It is generally observed that Na^+ ion conductivity prevails in solid Na_2SO_4 (235-883 C) and that the partial electronic conductivity is negligible. Thus the electrode for the potentiostatic polarization cell was chosen to be reversible with respect to the cation (Na^+) present in the molten sodium sulfate. If the cation reversible electrode works properly, then complete cell polarization is expected when the anion diffusion, created by a salt gradient, exactly opposes the migration of this ion under the influence of the applied potential.

The cationic transport numbers are displayed as a function of Na_2O activity in the melt in Figure 6. It is clear from this figure that the molten Na_2SO_4 is an ionic conductor ($t_{Na^+} = 0.98$). However, this result shows that the cationic transport numbers are decreased in the low sodium oxide activity region of the melt. In another words, the contribution of the possible anion species such as SO_4^{--}, $S_2O_7^{--}$ or O^{--} is not negligible in such a region of the melt.

(ii) Na_2SO_4 melt containing Cr_2O_3

The studies for the role of alloying elements upon influencing hot corrosion have shown a general agreement to the beneficial role of chromium in reducing hot corrosion. Superalloys containing relatively high concentrations of chromium have good resistance to hot corrosion attack due to the formation of a protective Cr_2O_3 scale at high temperatures. However, the hot corrosion rate is still too high to provide a reasonable lifetime for superalloys in environments containing sulfur. In addition, a Cr_2O_3 scale is soluble in a

Na_2SO_4 melt to some degree[48] and the chromium oxide has been shown to react with molten Na_2SO_4 as indicated by chemical analyses of the water-wash solution[49]. A study of certain properties of molten sodium sulfate containing chromium oxide for elucidating the hot corrosion process was performed by the total electrical conductivity measurements as well as Wagner-Hebb type polarization experiments.

The total electrical conductivities of molten Na_2SO_4 containing 10^{-3} m/o, 10^{-2} m/o, 10^{-1}m/o and supersaturated (1 m/o) Cr_2O_3 measured by using an A.C. impedance method are displayed in Figure 7 as a function of Na_2O activity at 1173K. The total electrical conductivities remain rather constant regardless of the changes in Na_2O activities in the melt. However, it is noted that the addition of Cr_2O_3 into the melt decreases the total conductivity systematically as compared to that of a pure Na_2SO_4 melt (Figure 3).

The electronic conductivities from the Wagner-Hebb type experiments in molten sodium sulfate containing chromium oxide have been obtained and are shown in Figures 8-11 as a function of Na_2O activity. The additions of Cr_2O_3 into the melt increase the electron hole conductivities and decrease the electron conductivities as compared to that of a pure Na_2SO_4 melt (Figure 4). The electron hole conductivities in molten Na_2SO_4 containing 10^{-3} m/o, 10^{-2} m/o, and 10^{-1}m/o Cr_2O_3 remain rather constant over the entire Na_2O activity range; however, the electron conductivities are slightly increased with decreasing Na_2O activities. This can be interpreted by means of thermodynamic anticipations.

The commercial SOLGASMIX program was utilized to calculate the thermodynamic activities of stable species in the melt at 1173 K and the experimental atmospheres. The thermodynamic data used in this calculation are mostly from the JANAF thermochemical tables (third edition,1985) except free energies for the formations of Na_2CrO_4 (l) [50], $NaCrO_2$ (s) [51] and $Cr_2(SO_4)_3$ (s) [52].

Figure 12 shows the activity changes of stable species in the melt containing 10^{-3} m/o Cr_2O_3 as a function of sodium oxide activity at 1173 K. In this figure, the activities of

only Cr_2O_3, Na_2CrO_4 and Na_2SO_4 was considered since the activities of other solute species are negligible at the given temperature and partial pressure of O_2 and SO_2. As the sodium oxide activity in the melt decreases, the activity of Cr_2O_3 increases significantly then decreases, and the activity of Na_2CrO_4 remains rather constant then decreases as shown in Figure 12. The activity of Na_2SO_4 does not show significant changes throughout the Na_2O activities in the melt. However,as the activities of Cr_2O_3 and Na_2CrO_4 decrease, the activity of Na_2SO_4 increases relatively as the Na_2O activities in the melt decreases. As it is noted from the Wagner-Hebb type polarization experiment on pure Na_2SO_4 melt, the electron conductivity was shown to be much greater than the electron hole conductivity over the entire range of Na_2O activities as shown in Figure 4. Thus, as the melt goes to the low Na_2O activity region, the electron conductivity increases as shown in Figure 8.

As the amount of Cr_2O_3 in the melt increases, the activity of Cr_2O_3 increases by two orders of magnitude while the activity of Na_2CrO_4 increases by about one order of magnitude as depicted in Figure 13. Thus, it is anticipated that the contribution of two solute species to the electronic conductivity in the melt containing 10^{-2} m/o Cr_2O_3 is comparable in the low Na_2O activity region. The fluctuations that appeared in the electron conductivity in Figure 9 is probably due to this reason. However, the increase in electron conductivity is due to the relative increase in Na_2SO_4 activity as the activity of Na_2O decreases.

The activity changes of Cr_2O_3, Na_2CrO_4 and Na_2SO_4 in the melt containing 10^{-1} m/o Cr_2O_3 is shown in Figure 14 as a function of Na_2O activity at 1173 K. The changes in those activities have same trends as in the other melts. The increase in the relative activity of molten Na_2SO_4, whose major minor defect is known to be electrons, may cause the increase in the electron conductivity at the low Na_2O activities.

Figure 15 describes the activity changes of stable species in the melt containing 1 m/o Cr_2O_3, calculated by the computer program, as a function of Na_2O activity at 1173 K. The activities of solute species are comparable to each other at low Na_2O activity

region. However, it is noted that the differences in the activities of Cr_2O_3, Na_2CrO_4 and Na_2SO_4 are getting smaller. Thus, the electron conductivities show some fluctuations. The magnitude of electron hole conductivity is increased in the melt containing 1 m/o Cr_2O_3 as compared to other melts since the activity of Cr_2O_3, which is known to have a p-type defect structure at the temperature and atmosphere of interest, is increased.The electron conductivity is increased while the electron hole conductivity is decreased at -log(sodium oxide activity) = 14. It is because the concentrations of 10^{-3} m/o, 10^{-2} m/o, and 10^{-1}m/o Cr_2O_3 are completely soluble in the melt throughout the Na_2O activity range while Cr_2O_3 would precipitate out at -log(sodium oxide activity) = 14 in the melt containing supersaturated (1 m/o) chromium oxide.

Combining the values of the electronic conductivities and total conductivities provide the transport numbers of electronic species in the melt as shown in Figures 16-19 for molten Na_2SO_4 containing 10^{-3} m/o, 10^{-2} m/o,10^{-1}m/o and supersaturated (1 m/o) Cr_2O_3 respectively. These figures emphasize that the partial electronic conductivities in the melts containing Cr_2O_3 are comparable each other, but the major species contributing to the electronic conduction are the electrons as compared to those of a pure Na_2SO_4 melt. The increase in transport numbers of electronic species in the low Na_2O activity range in such melts resulted from the increase in electronic conductivities in the same range.

(iii) **Vanadium and Zirconia Experiments**

(a) Thermodynamic Modelling

SOLGASMIX was used to simulate the Al_2O_3-V_2O_5-Na_2SO_4 and stabilized zirconia-V_2O_5-Na_2SO_4 systems. Using this program, the activity of V_2O_5 showed no dependence on temperature (Fig.20) until T > 1700 K (above the temperatures found in a gas turbine). This implies that in a vanadium attack reaction; the reactivity of V_2O_5 is uneffected by temperature. Using this data as an assumption, one could then conclude that a change in corrosion mechanism as temperature is increased is not caused by a change in

V_2O_5 activity. In Fig.21-22, the activities of CaO and ZrO_2 are plotted versus temperature (at 10 ppm V_2O_5 and $P_{O2} = 10^{-5}$) and oxygen partial pressure (at 10 ppm V_2O_5 and 1000 K). In Fig. 21, the activity of CaO appears independent of temperature, and, only at high temperatures, does the zirconia activity change even slightly. In Fig. 22, neither activity has any apparent dependence on oxygen activity. It is critical to note that these results are from very simplified models; more complex thermodynamic models of the hot corrosion of zirconia are not yet complete.

Alumina samples which were exposed to V_2O_5 (.1-2 wt% of the sample) at 1273 K for 200 hours showed no evidence of surface corrosion while evidencing a significant solubility for the vanadium compound. This result was not expected because past literature has detailed examples of vanadic attack on alumina. Hot corrosion experiments on 4.5 and 8 wt% Y_2O_3 stabilized zirconia held at 973 and 1173 K with similar concentrations of V_2O_5 exhibited very different behavior. In runs only 24 hours long, significant corrosive damage occurred. These results were in agreement with the work of others. More detailed studies involving V_2O_5, $NaVO_3$, and Na_2SO_4 are ongoing and,with the addition of electrical measurements, should aid in revealing a mechanism for the hot corrosion of zirconia.

The aforementioned electrical conductivity measurements are also in the preliminary stages. By the nature of these experiments, it is important to have fully dense samples; however, samples which are not fully dense can still be of use. In Table 1, the compositions, the conductivities, and the densities of a number of stabilized zirconia samples are listed. There exists only a slight dependence of conductivity upon porosity. Current experiments are examining the effects of grain boundaries on conductivity and the role of ionic transport in hot corrosion mechanisms.

V. SUMMARY AND CONCLUSION

The main thrust of this experimental program was to obtain some of the transport properties in the aggressive molten salt Na_2SO_4. The total electrical conductivity measurements by an A.C. impedance technique and Wagner-Hebb type polarization experiments provided the total electrical conductivity, electron conductivity, and electron hole conductivity of a pure Na_2SO_4 melt at 1173 K. From these measurements the transport numbers of electrons, $t_\ominus$, and electron holes, $t_\oplus$, were calculated as follows:

$$t_\ominus = 5.6 \times 10^{-3}\ ; \qquad t_\oplus = 1.6 \times 10^{-4}$$

Such experimental investigations show that the pure Na_2SO_4 melt had a somewhat low total electrical conductivity and the electronic conduction occurs primarily via the transport of electrons.

The cationic transport numbers of pure Na_2SO_4 melt was obtained by utilizing the potentiostatic polarization technique. The result indicates that the pure Na_2SO_4 melt is a cationic conductor over a wide range of Na_2O activities at 1173 K.

Unlike the behavior of NiO in the Na_2SO_4 melt the dissolution of Cr_2O_3 at the concentration levels of 10^{-3} *m/o*, 10^{-2} *m/o*, 10^{-1} *m/o* and 1 *m/o* has significant changes on the electronic conductivities of the melt. The melts containing Cr_2O_3 showed increased electron hole conductivity and decreased electron conductivity as compared to pure the Na_2SO_4 melt. Additionally, the dissolved Cr_2O_3 decreased the total electrical conductivity of the Na_2SO_4 melt.

Vanadium hot corrosion was studied on two ceramic coating materials, alumina and stabilized zirconia. In situ V_2O_5 attack experiments showed significant solubility of V_2O_5 in Al_2O_3 while apparently causing little surface corrosion of the alumina. Similar work with stabilized zirconia samples evidenced definite corrosive dissolution of the surface.

Electrical conductivity measurements showed that conductivity is a function of percent of total density although the dependence is not very strong. Thermodynamic models of both the Al_2O_3 -Na_2SO_4-V_2O_5 and the stabilized zirconia-Na_2SO_4-V_2O_5 systems described very simple systems. The results are accurate within these systems, but more complex models are required to draw definite conclusions

REFERENCES

1. J.M. Quets and W.H. Dresher, Nuc. Mat., 14, 583 (1969)

2. N.S. Bornstein, M.A. DeCrescente, Met. Trans., 2, 2875 (1971)

3. J.A. Goebel and F.S. Pettit, Met. Trans.,1, 1943 (1970)

4. J.A. Goebel, F.S. Pettit, and G.W. Goward, Met. Trans., 4 , 261 (1973)

5. R.A. Rapp and K.S. Goto, "Proceedings of Second International Symposium on Molten Salts", J.Braunstein and J.R. Selman eds., Electrochem. Soc. p159 (1981)

6. C. Wagner, Proc. of Seventh Meeting of the Inter. Comm. on Thermo. and Kinetics of Electrochem. (CITCE), Butterworth Scientific Publications, London, Vol. 7, p. 361 (1957).

7. M. H. Hebb, J. Chem. Phys., 20, 185 (1952).

8. Luthra, K. and H. Spacil, J. Electrochem. Soc., 129, 3, 649-656, 1982.

9. Jones, R. L., Low Quality Fuel Problems With Advanced Materials, NRL Report 6252, August 1988.

10. Kroger, F. A., Chemistry of Imperfect Crystals, Wiley, New York, 1964, p.194.

11. Su, M. Y., Point Defect Structure of Chromium Sesquioxide, PhD thesis, Penn State Univ., 1987, p.4-6.

12. Liebert, C., R. Jacobs, S. Stecura, and C. Morse, "Durability of Zirconia Thermal Barrier Coatings on Air Cooled Turbine Blades in Cyclic Jet Engine Operation", NASA TM X-3410, Sept. 1976.

13. Sevcik, W. and B. Stoner, "Analytical Study of Thermal Barrier Coated First-stage Blades In a JT9D Engine", NASA CR-135360, Jan. 1977.

14. Carlson, N. and B. Stoner, "Study of Termal Barrier Coatings on High Temperature Industrial Gas Turbine Engines", NASA CR-135147, Feb. 1978.

15. Subbarao, E. C., "Zirconia an Overview", Science and Technology of Zirconia, Advances in Ceramics Vol. 3, ed, by Heuer, A. H. and L. W. Hobbs, Amer. Cer. Soc., 1981, p. 1-24.

16. Wolten, G. W., J. Amer. Cer. Soc., 46, 9, 418-22, 1963.

17. Stubican, V. S. and J. R. Hellmann, "Phase Equilibria in Some Zirconia Systems", Science and Technology of Zirconia, Advances in Ceramics Vol. 3, ed, by Heuer, A. H. and L. W. Hobbs, Amer. Cer. Soc., 1981, p.25-36.

18. Patton, J. S. and R. L. Clarke, "Hot Corrosion Resistance of Yttria-Stabilized Zirconia Coatings", 1989 Tri-Service Corrosion Conference, 1989.

19. Nagelberg, A. S., J. Electrochem. Soc., 132, 2502, 1985.

20. Jones, R. L., and C. E. Williams, J. Electrochem. Soc., 132, 1498, 1985.

21. Jones, R. L., and C. E. Williams, J. Electrochem. Soc., 133, 227, 1986.

22.Singhal, S. and R. J. Bratton, "Stability of a ZrO2(Y2O3) Thermal Barrier Coating in Turbine Fuel with Contaminant", J. Eng. for Power, 102, 4 , 770-775, 1980.

23. Palko, J., K. Luthra, and D. McKee, "Evaluation of performance of Thermal Barrier Coatings Under Simulated Industrial/Utility Gas Turbine Conditions", Final Report, General Electric Co.,1978.

24. Zaplatynsky, I., "Reactions of Yttria-Stabilized Zirconia with Oxides and Sulfates of Various Elements", DOE/NASA/2593-78/1, NASA TM-78942, 1978.

25. J.E.B. Randles, Dis. Faraday. Soc., 1, 11 (1947)

26. G.W. Walter, Corr. Sci., 26, 681 (1986)

27. F. Mansfeld, Corr.-NACE, 36, 301 (1981).

28. J. B. Wagner, Jr. and C. Wagner, J. Chem. Phys., 26, 1597 (1957).

29. A. Lingras and G. Simkovich, J. Phys. Chem. Solids, 39, 1225 (1978).

30. A. V. Joshi and J. B. Wagner, Jr., J. Phys Chem. Solids, 33, 205 (1972).

31. A. V. Joshi and J. B. Wagner, Jr., J. Electrochem. Soc., 122, 1071 (1975).

32. D. Raleigh, J. Phys. Chem. Solids, 26, 329 (1965).

33. J. Sachoonman, A. Wolfert, and D. F. Untereker, Solid State Ionics, 11, 187 (1983).

34. R. J. Heus and J. J. Egan, J. Phys. Chem., 77, 1989 (1973).

35. R. J. Heus and J. J. Egan, in "Proceedings of International Symposium on Molten Salts," Electrochem. Soc., Pennington, NJ (1976), p. 523.

36. G. J. Reynolds, M.C.Y. Lee and R. A. Huggins, in "Proceedings of the Fourth International Symposium on Molten Salts," Electrochem. Soc., pv 84-2, Pennington, NJ (1984), p. 519.

37. D.F. Shriver, S. Clancy, P.M. Blonsky, and L.C. Hardy, "Sixth Risφ International Symposium on Met. and Mat. Sci." p353 (1985)

38. D.H. Kim and G. Simkovich, "Proceedings of Symposium on High Temperature Materials Chemistry IV", Ed. Z.A. Munir, D. Cubicciotti, and H. Tagawa, Electrochem Soc. 88-5, p26 (1988)

39. D. A. Shores and R. C. John, J. Appl. Electrochem. 10, 275 (1980).

40. D. Dobos, "Electrochemical Data," Elsevier Scientific Publishing Co., New York, p. 57 (1975).

41. R.J. Labrie and V.A. Lamb, J. Electrochem. Soc., 106, 895 (1959)

42. H. Schmalzreid, Z. Phys. Chem. (Frankfurt), 38, 87 (1963)

43 A. Kvist, Z. Naturforschg., 22a, 208 (1967).

44. A. Kvist, Z. Naturforschg., 22a, 467 (1967).

45. A. Josefson and A. Kvist, Z. Naturforsch, 24a, 466 (1969).

46. K. Matiasovsky, V. Danek, and B. Lillebuen, Electrochim. Acta, 17, 463 (1972).

47. R. J. Heus and J. J. Egan, J. Phys. Chem., 77, 1989 (1973).

48. Y.S. Zhang, J. Electrochem. Soc., 133, 165 (1986)

49. G.C. Fryburg, F.J. Kohl, C.A. Stearn, and W.L. Fielder, J. Electrochem. Soc., 129,571 (1982)

50. W.W. Liang and J.F. Elliott, J. Electrochem. Soc., 123, 617 (1976)

51. B.J. Shaiu, P.C.S. Wu, and P.Chiotti, J. Nucl. Mater., 67, 13 (1977)

52. K.T. Jacob, D.B. Rao, and H.G. Nelson, Metall. Trans., 10A, 327 (1979)

TABLE I

Composition	Conductivity (ohm-cm)x10^{-6}	% of full Density
16 wt% CeO_2-ZrO_2	5.21	67.4
16 wt% CeO_2-ZrO_2	5.20	69.14
20 wt% MgO-ZrO_2	4.10	67.25
20 wt% MgO-ZrO_2	5.00	69.83
4.5 wt% Y_2O_3-ZrO_2	4.41	88.6
4.5 wt% Y_2O_3-ZrO_2	4.89	92.02
8 wt% Y_2O_3-ZrO_2	4.58	91.48
8 wt% Y_2O_3-ZrO_2	4.51	89.06

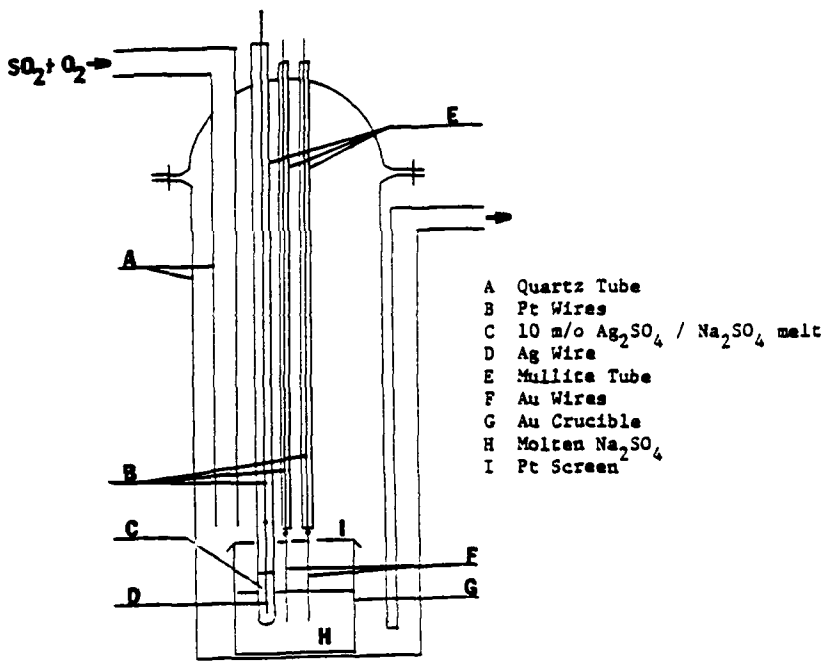

Figure 1. Schematic A.C. impedance cell arrangement

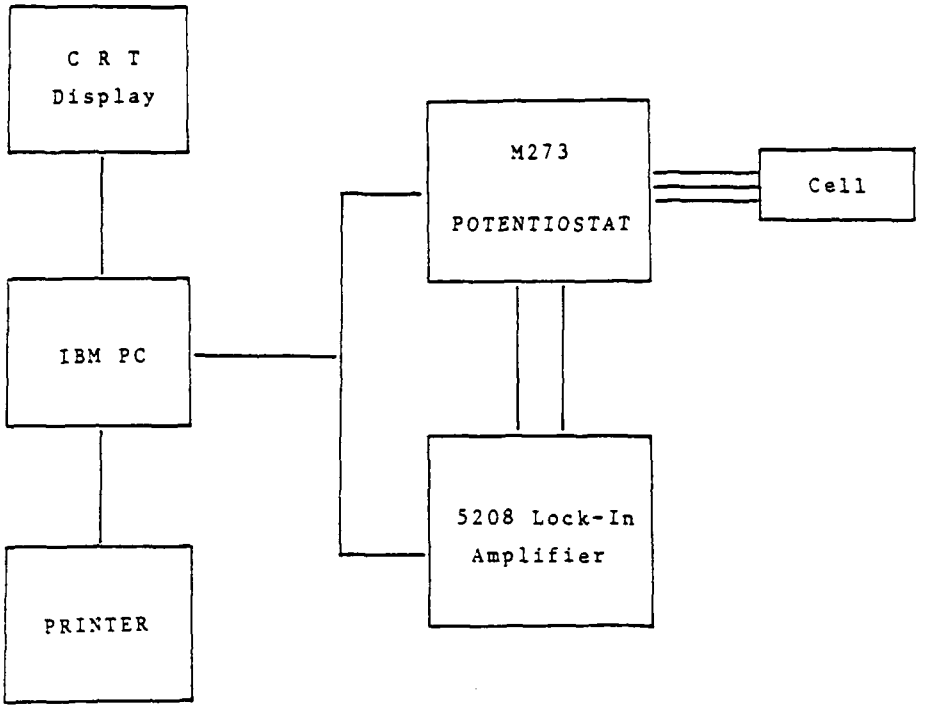

Figure 2. Schematic diagram of A.C. impedance experiment

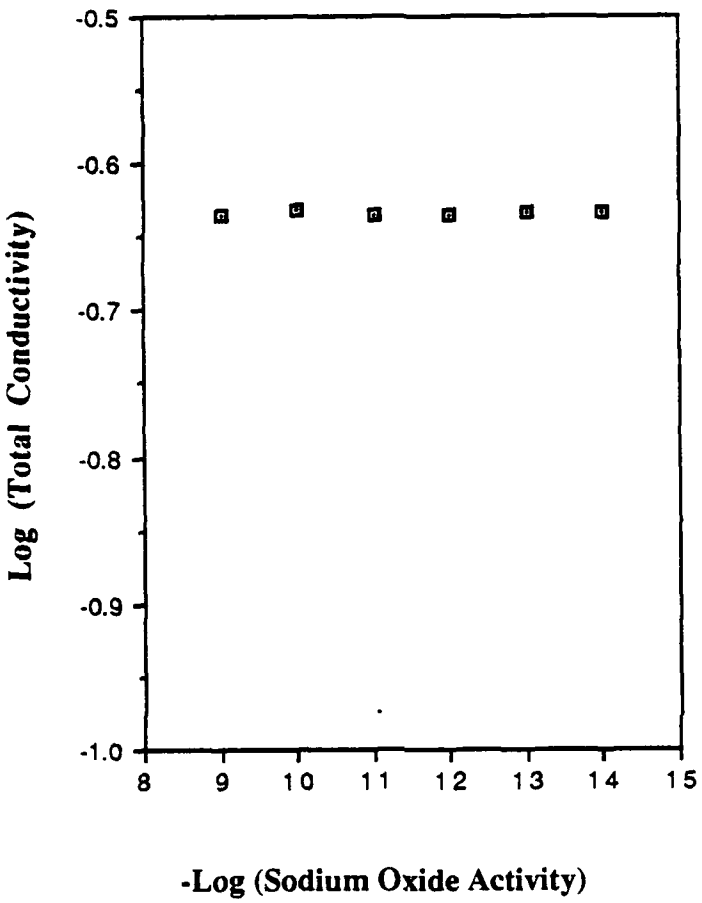

Figure 3. Log(total conductivity) versus Na_2O activity in a pure Na_2SO_4 melt at 1173K

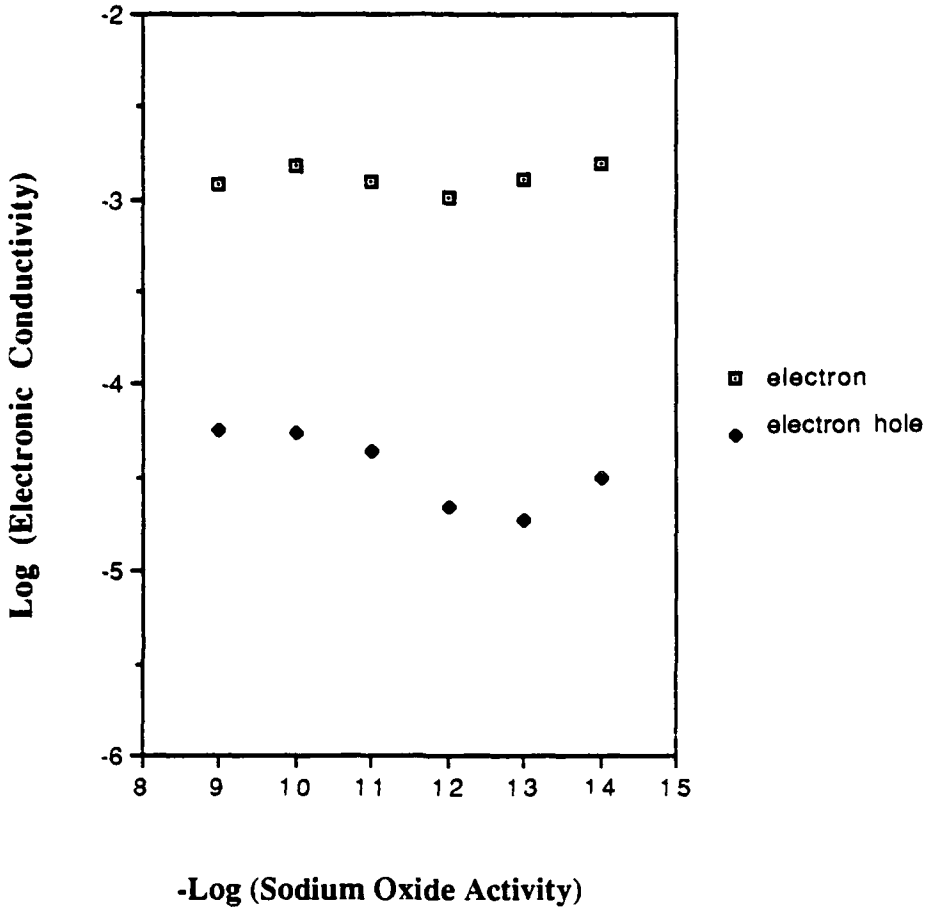

Figure 4. Electronic conductivities in a pure Na_2SO_4 melt as a function of Na_2O activity at 1173K

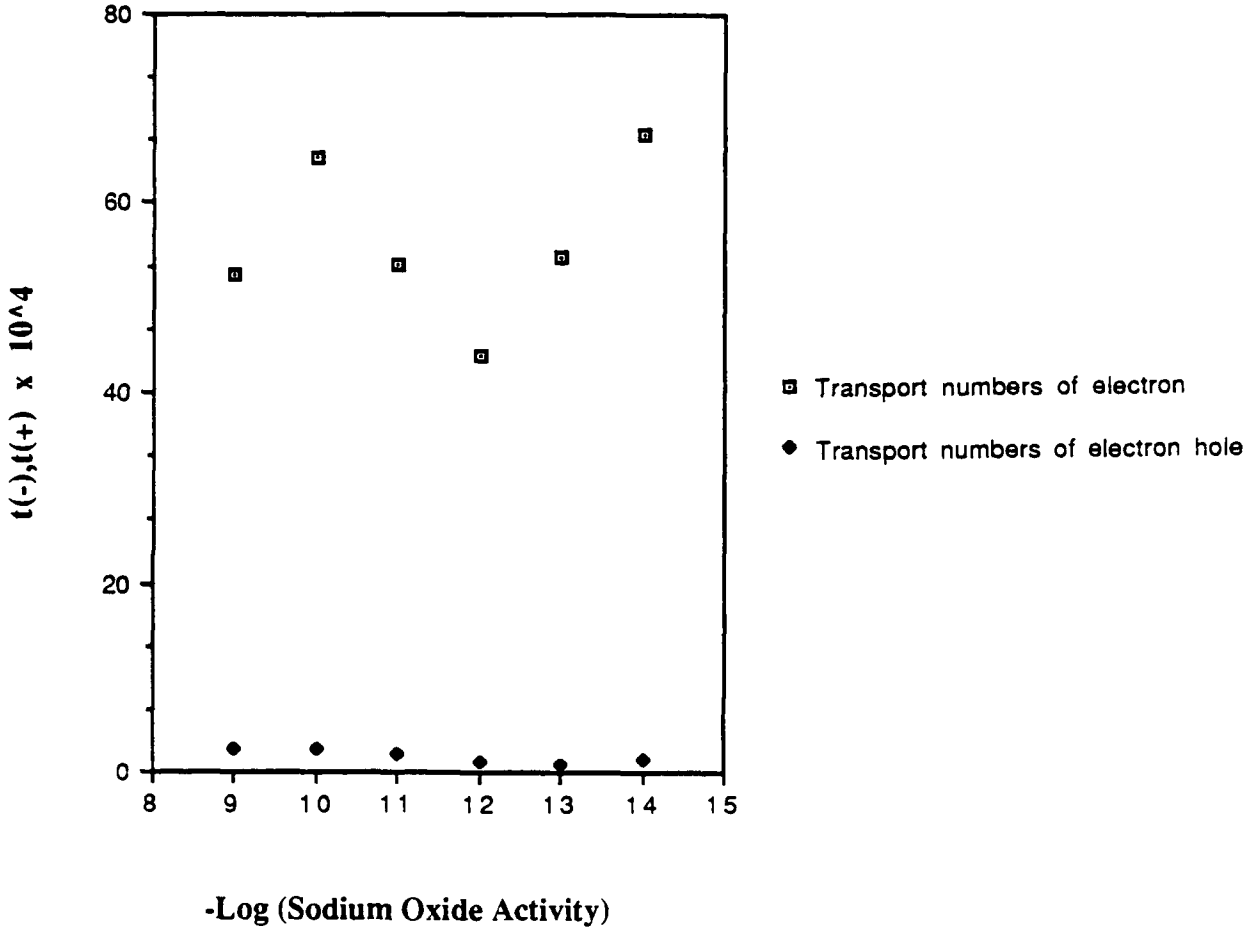

Figure 5. Transport numbers of electronic species in a pure Na_2SO_4 melt as a function of Na_2O activity at 1173K

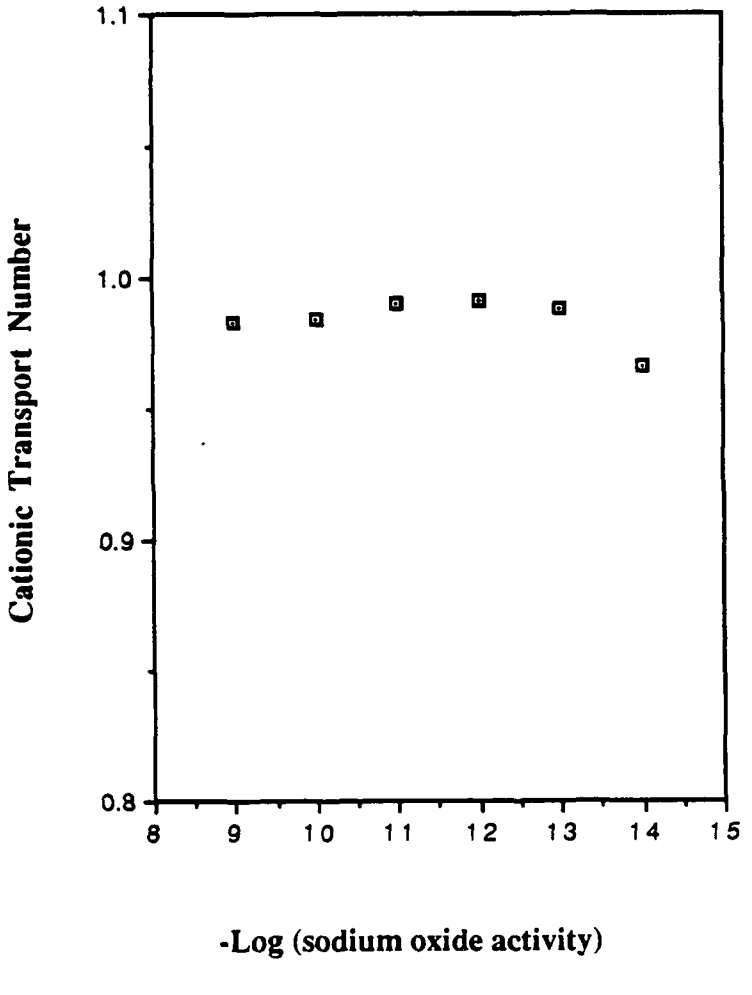

Figure 6. Cationic transport numbers of pure pure Na_2SO_4 melt as a function of Na_2O activity at 1173K

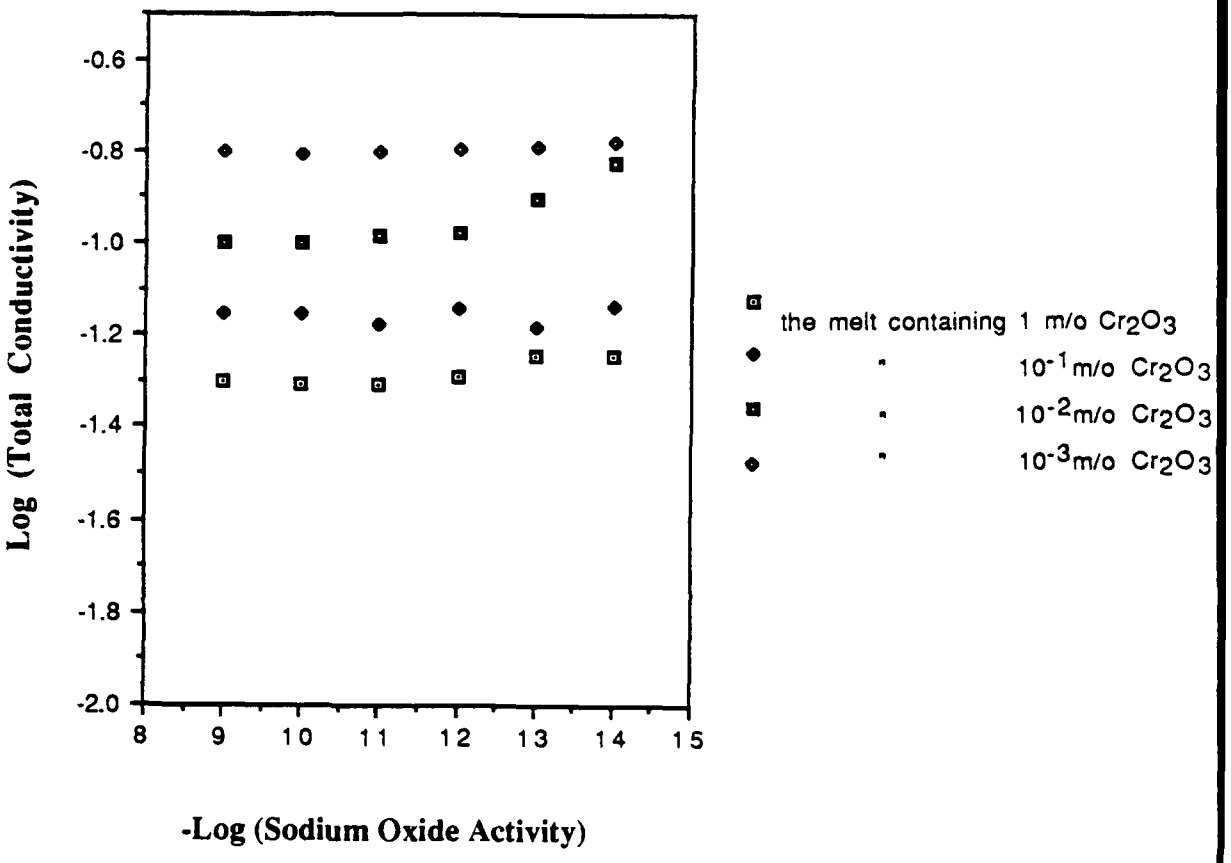

Figure 7. Log(total conductivity) versus Na_2O activity in a melt containing 10^{-3} m/o, 10^{-2} m/o, 10^{-1}m/o and supersaturated (1 m/o) Cr_2O_3 at 1173K

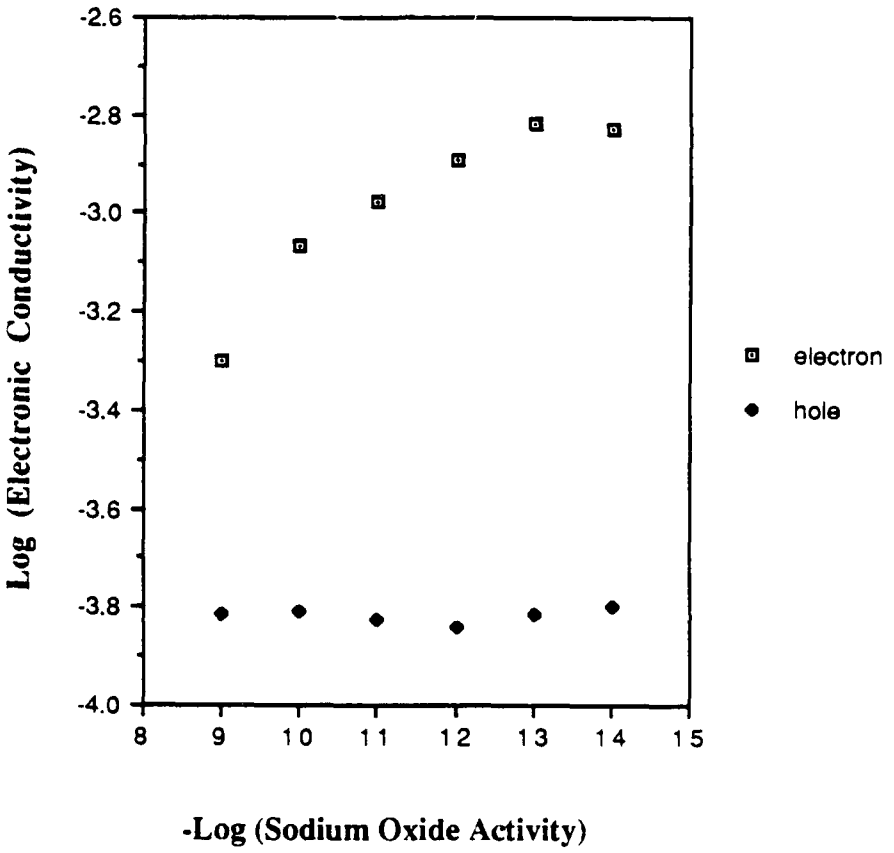

Figure 8. Electronic conductivities in a Na_2SO_4 melt containing 10^{-3} m/o Cr_2O_3 as a function of Na_2O activity at 1173K

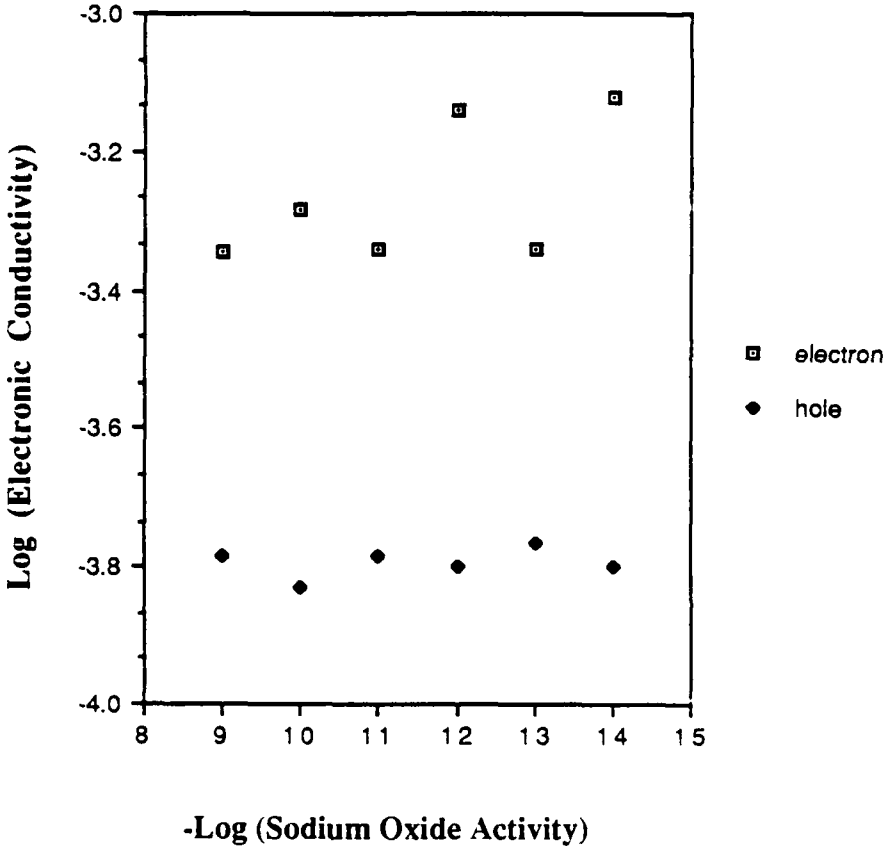

Figure 9. Electronic conductivities in a Na_2SO_4 melt containing 10^{-2} m/o Cr_2O_3 as a function of Na_2O activity at 1173K

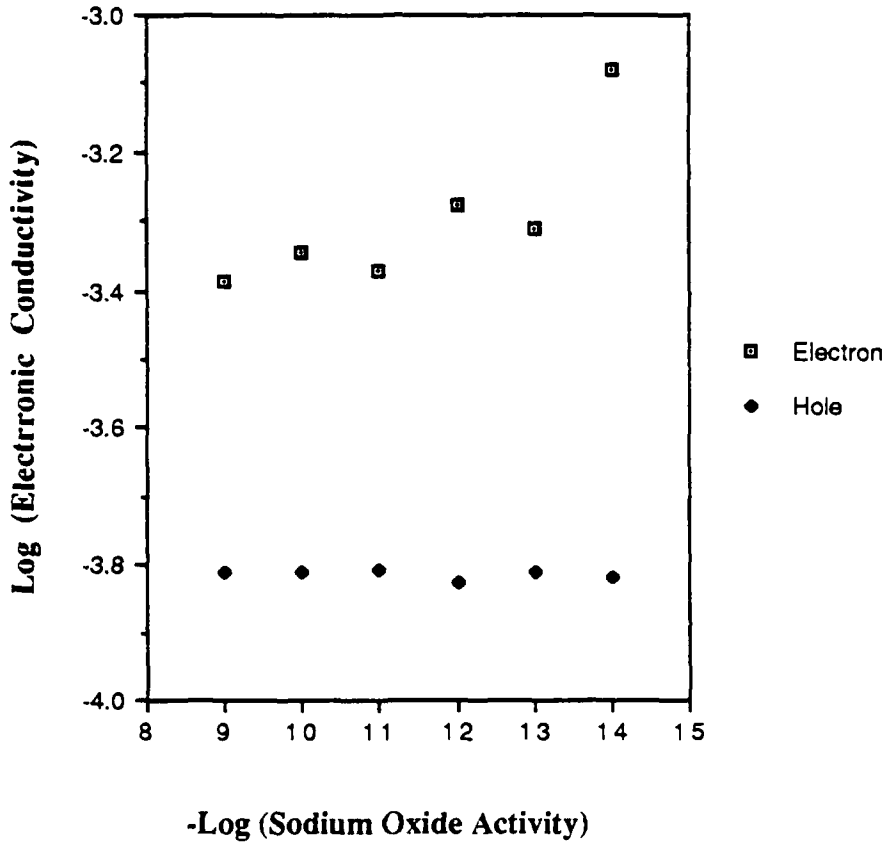

Figure 10. Electronic conductivities in a Na_2SO_4 melt containing 10^{-1} m/o Cr_2O_3 as a function of Na_2O activity at 1173K

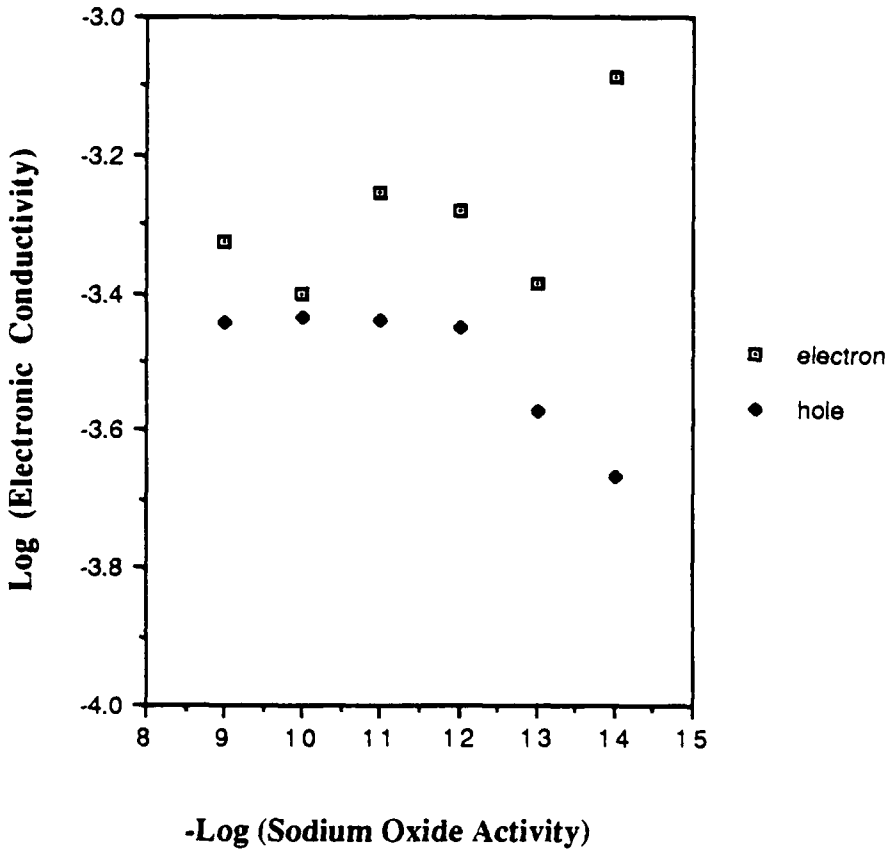

Figure 11. Electronic conductivities in a Na_2SO_4 melt containing supersaturated (1 m/o) Cr_2O_3 as a function of Na_2O activity at 1173K

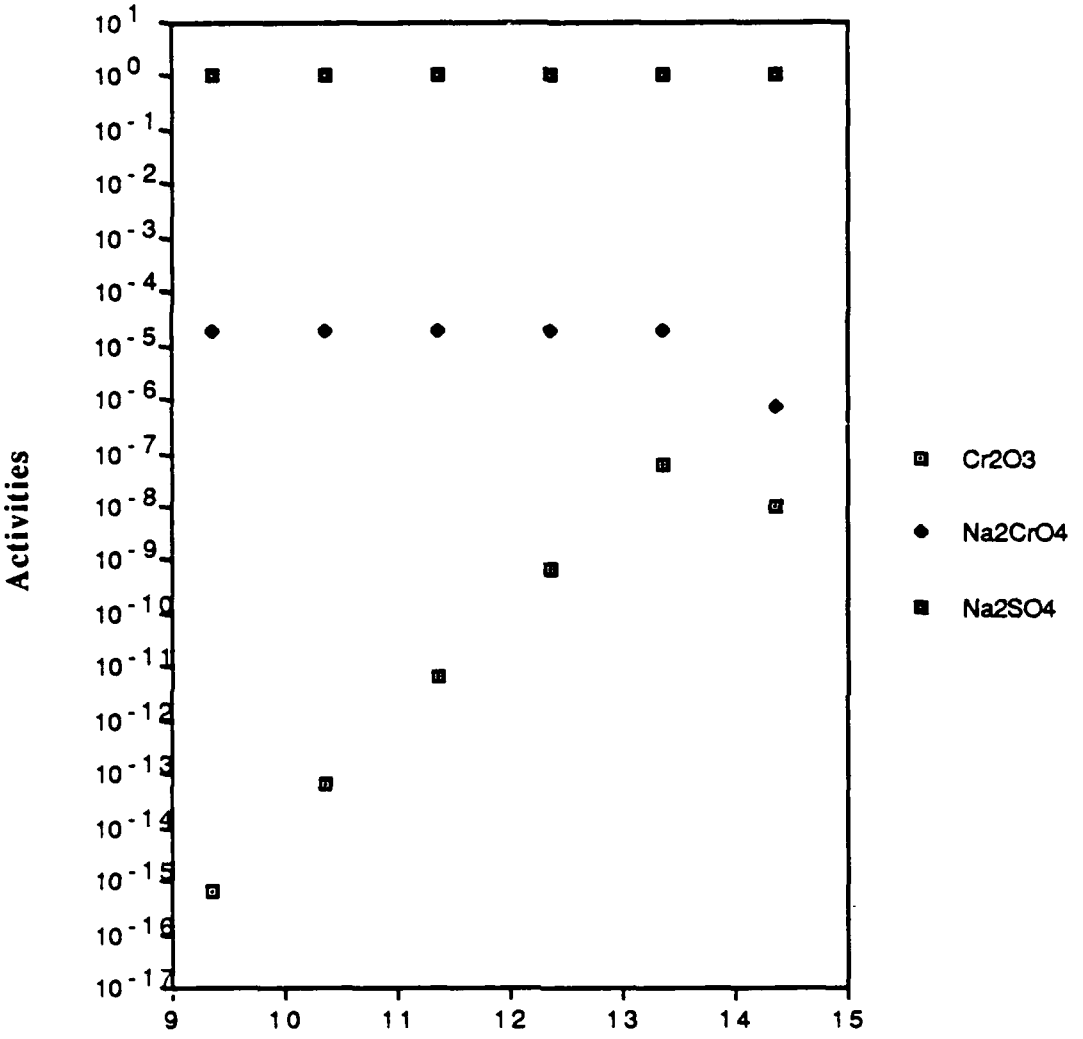

Figure 12. Activity diagram of stable species in a Na_2SO_4 melt containing 10^{-3} m/o Cr_2O_3 as a function of Na_2O activity at 1173K

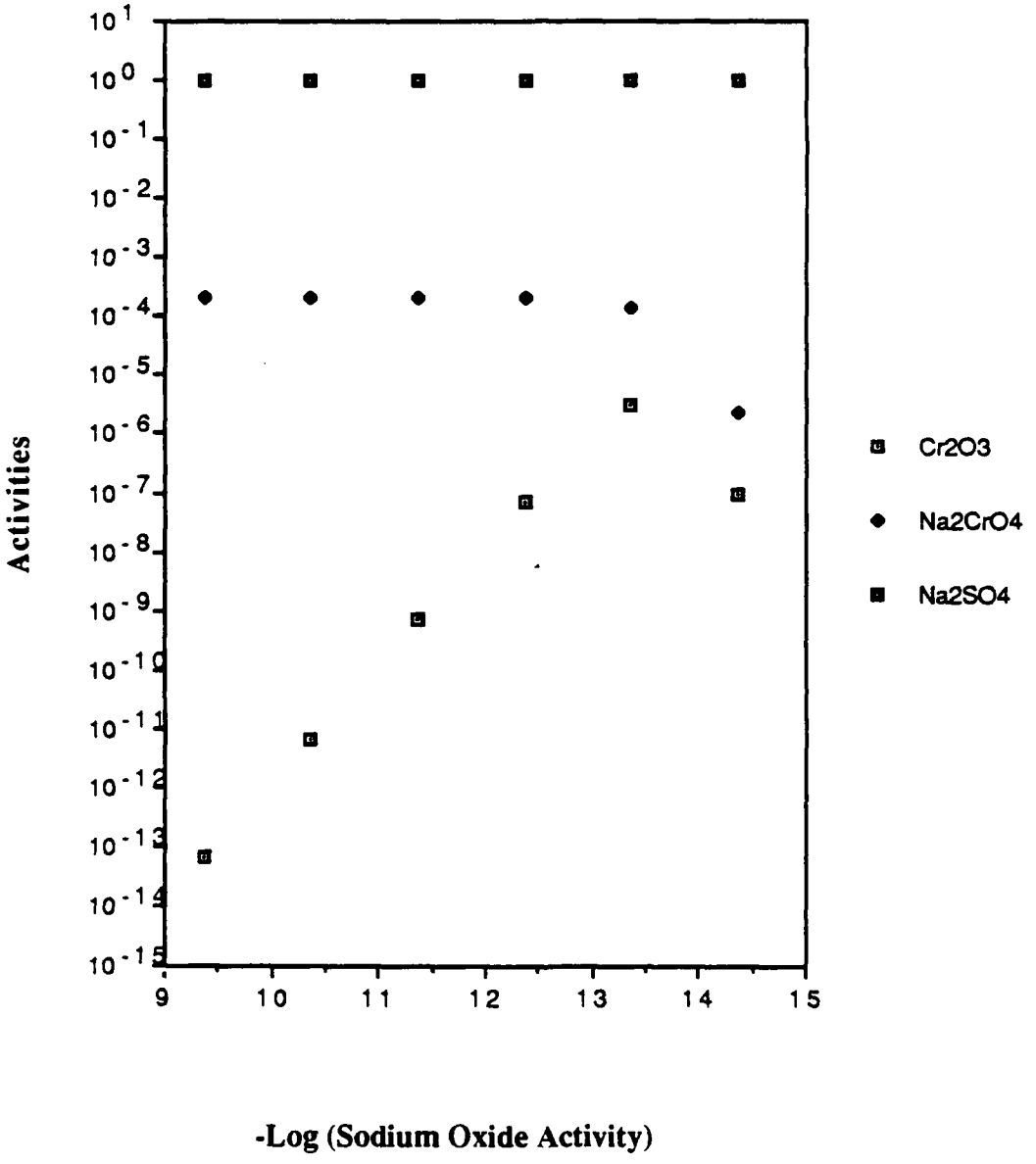

Figure 13. Activity diagram of stable species in a Na_2SO_4 melt containing 10^{-2} m/o Cr_2O_3 as a function of Na_2O activity at 1173K

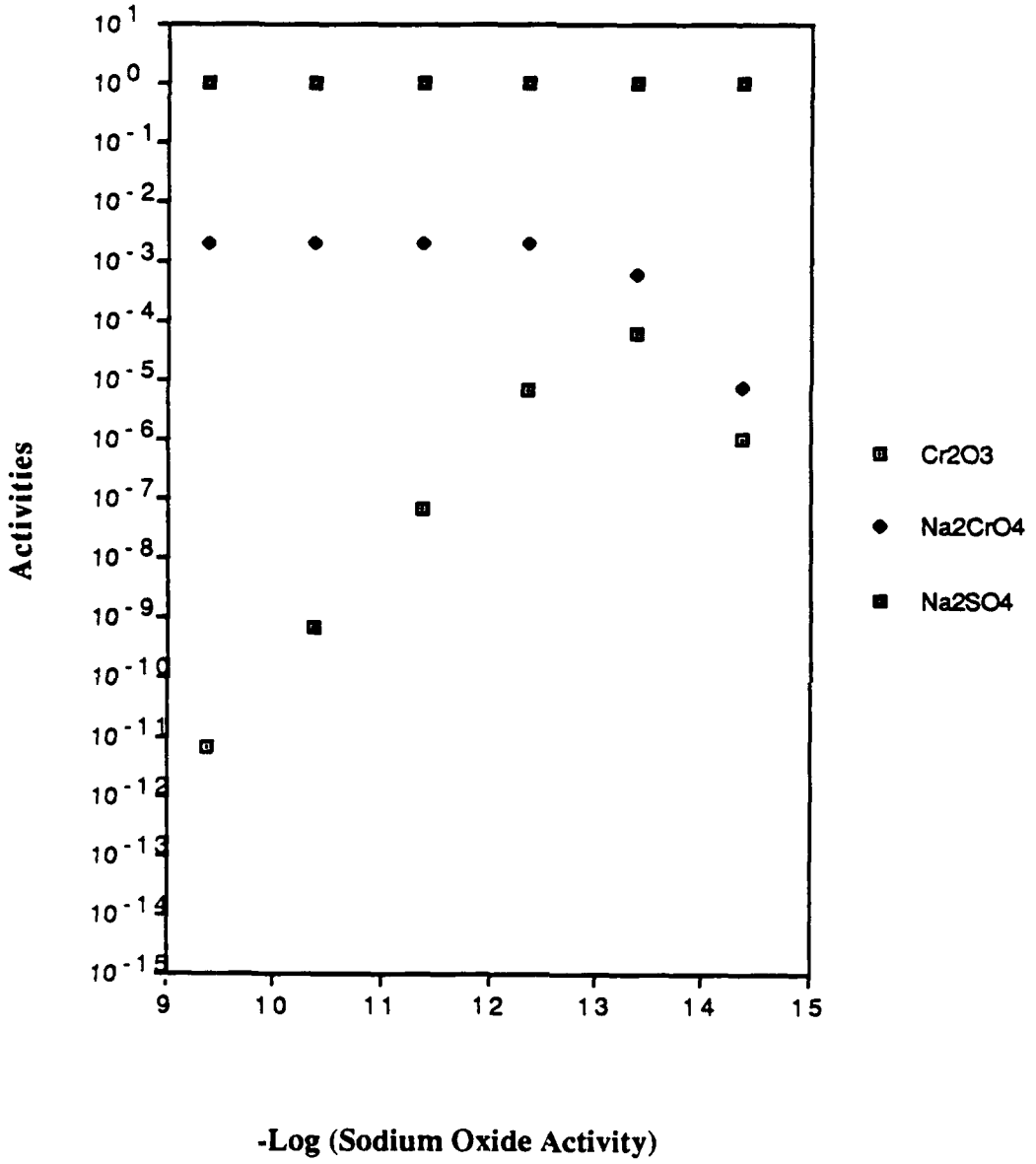

Figure 14. Activity diagram of stable species in a Na_2SO_4 melt containing 10^{-1} m/o Cr_2O_3 as a function of Na_2O activity at 1173K

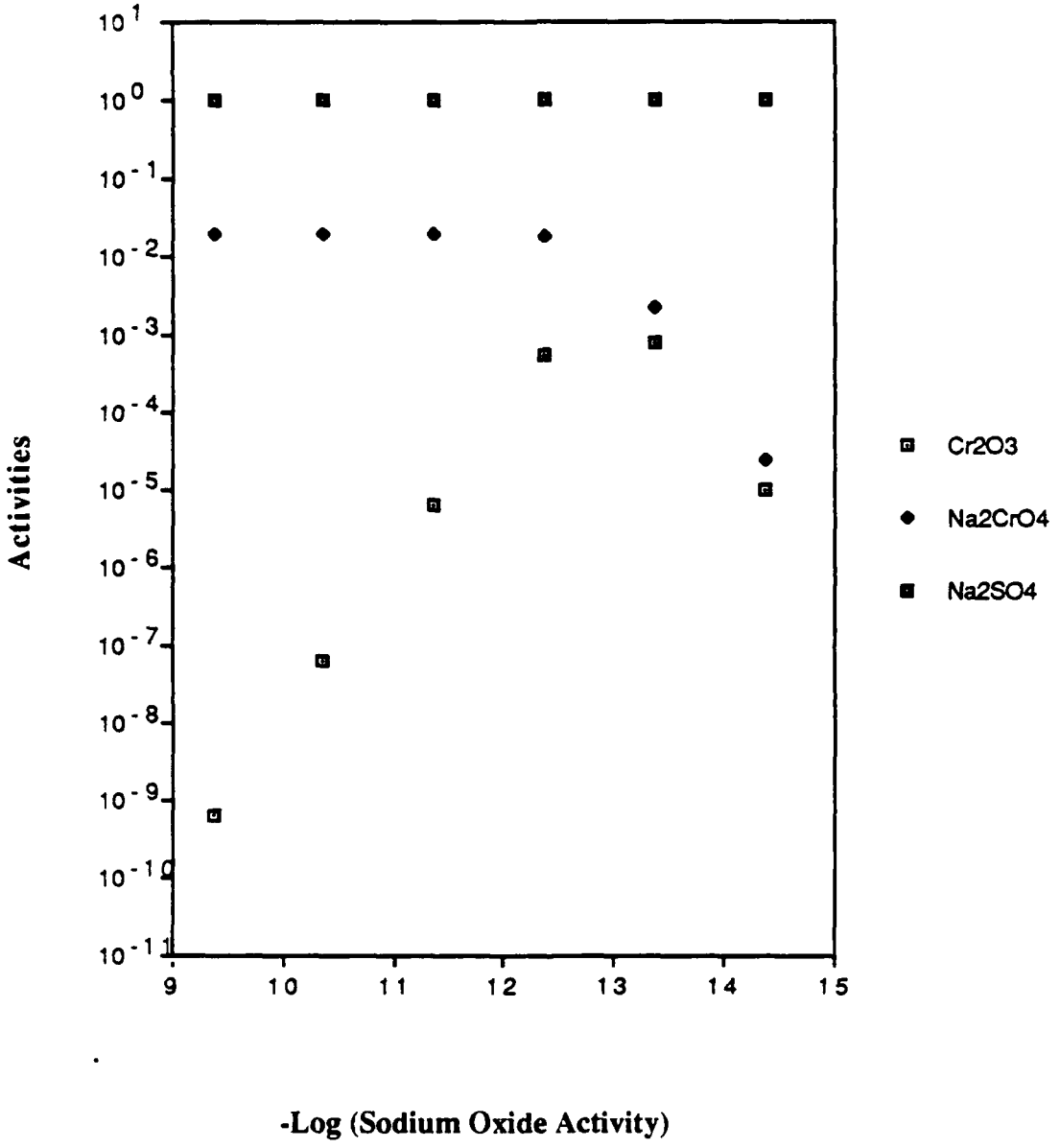

Figure 15. Activity diagram of stable species in a Na_2SO_4 melt containing supersaturated (1 m/o) Cr_2O_3 as a function of Na_2O activity at 1173K

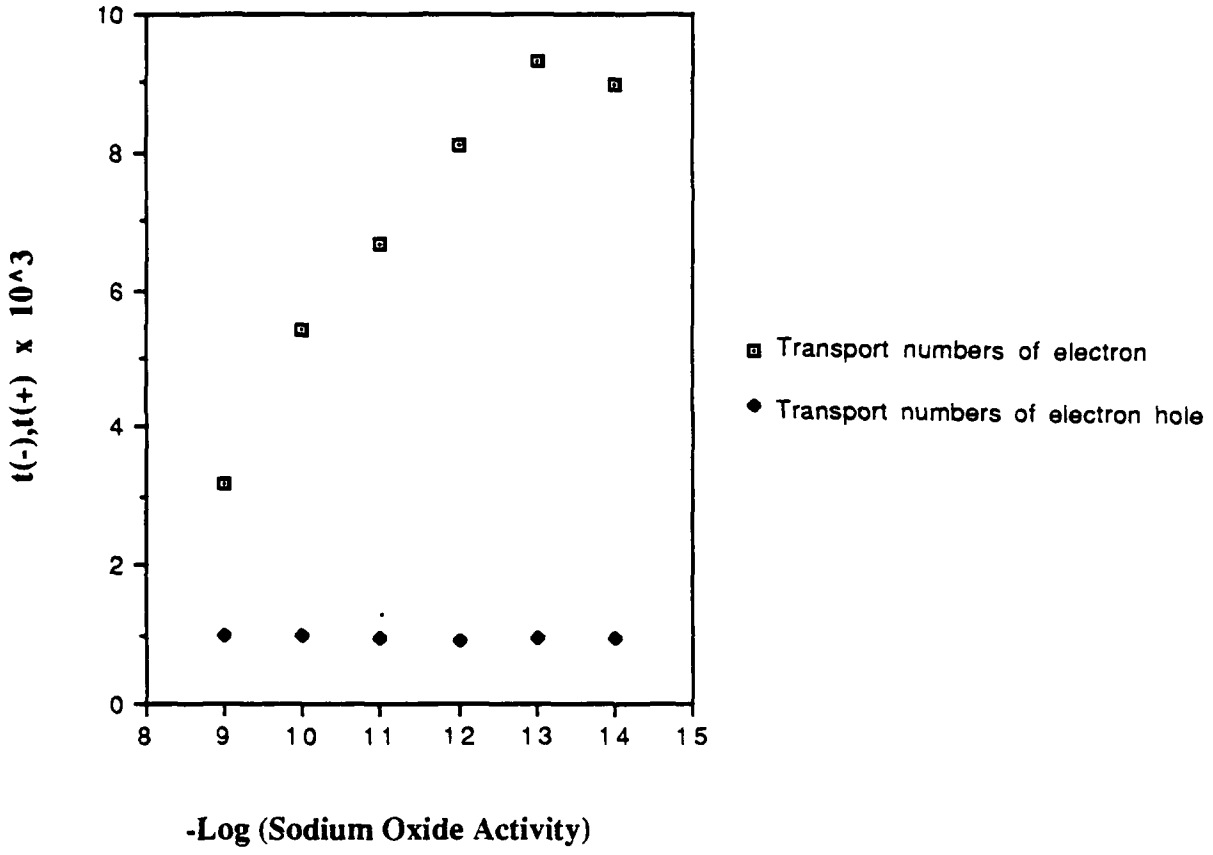

Figure 16. Transport numbers of electronic species in a Na_2SO_4 melt containing 10^{-3} m/o Cr_2O_3 as a function of Na_2O activity at 1173K

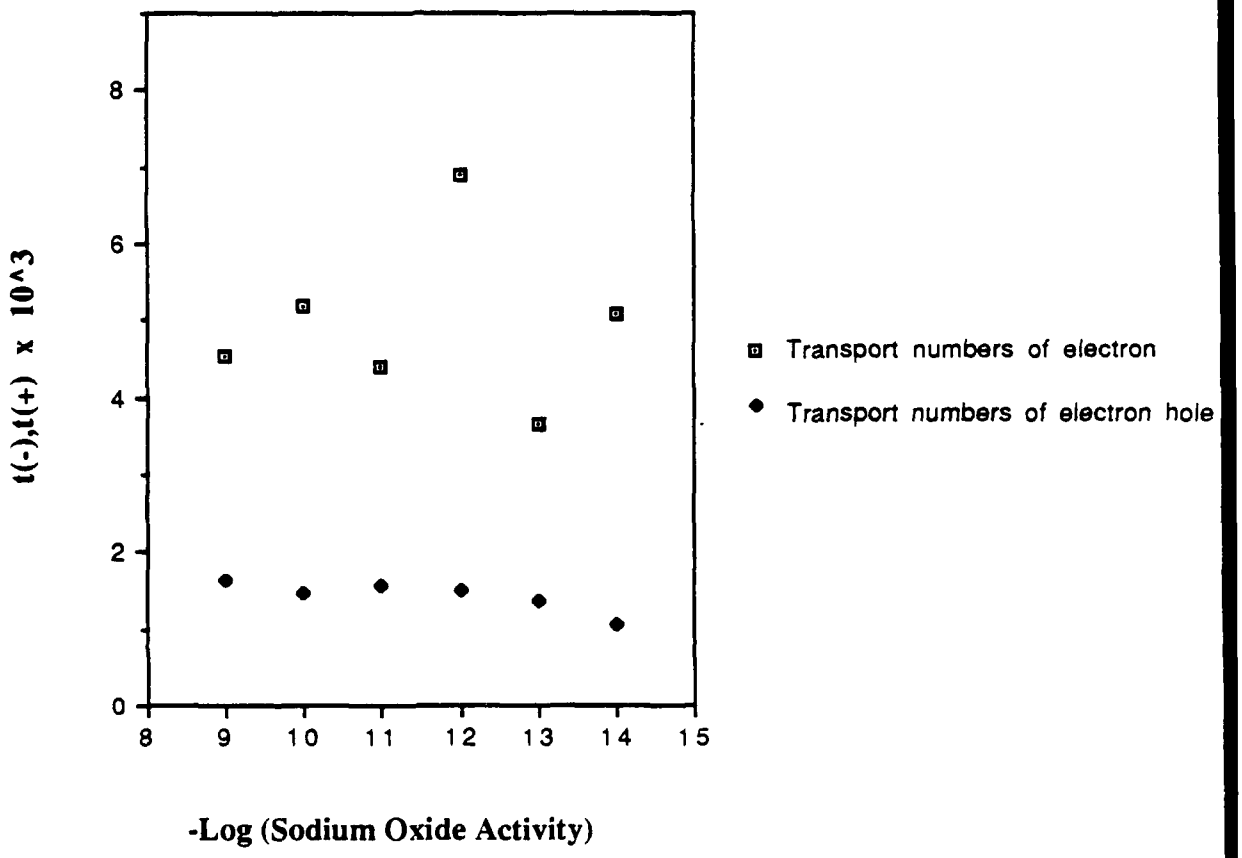

Figure 17. Transport numbers of electronic species in a Na_2SO_4 melt containing 10^{-2} m/o Cr_2O_3 as a function of Na_2O activity at 1173K

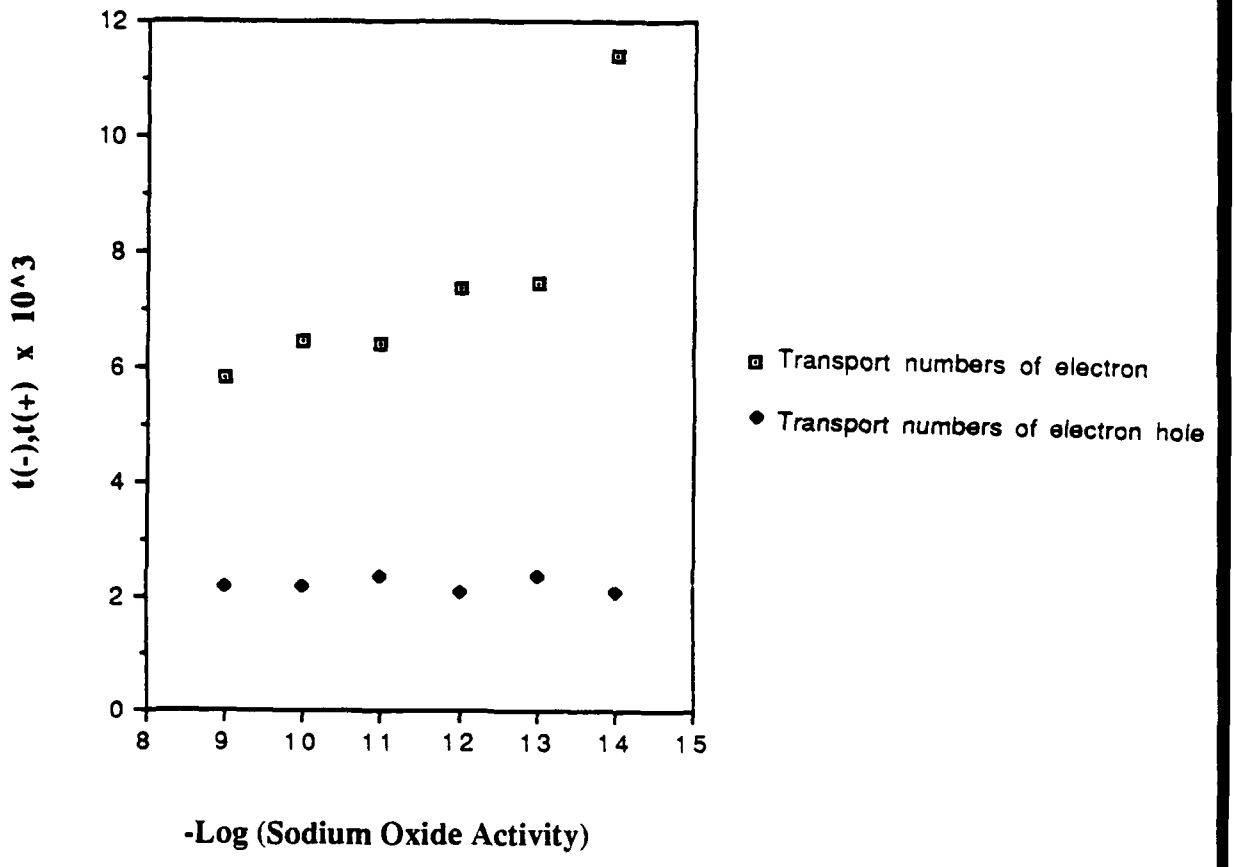

Figure 18. Transport numbers of electronic species in a Na_2SO_4 melt containing 10^{-1} m/o Cr_2O_3 as a function of Na_2O activity at 1173K

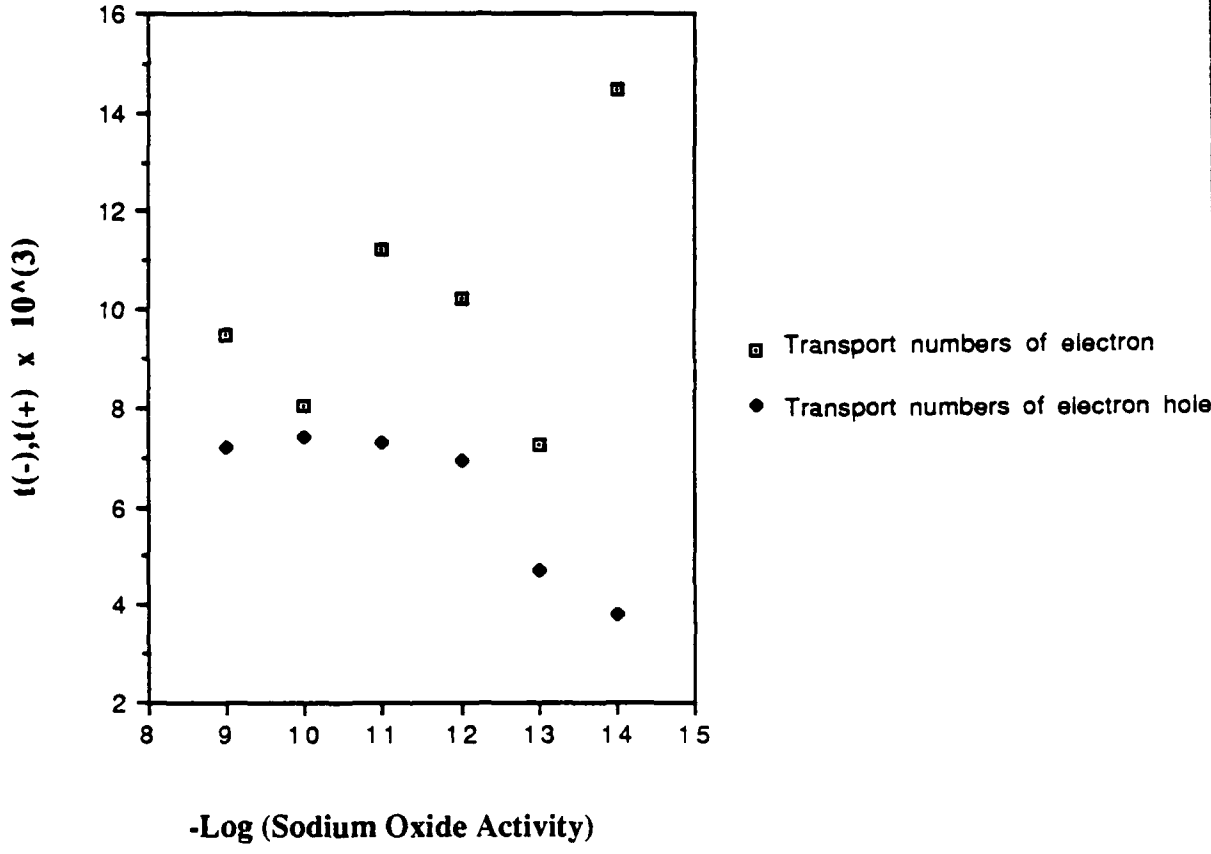

Figure 19. Transport numbers of electronic species in a Na_2SO_4 melt containing supersaturated (1 m/o) Cr_2O_3 as a function of Na_2O activity at 1173K

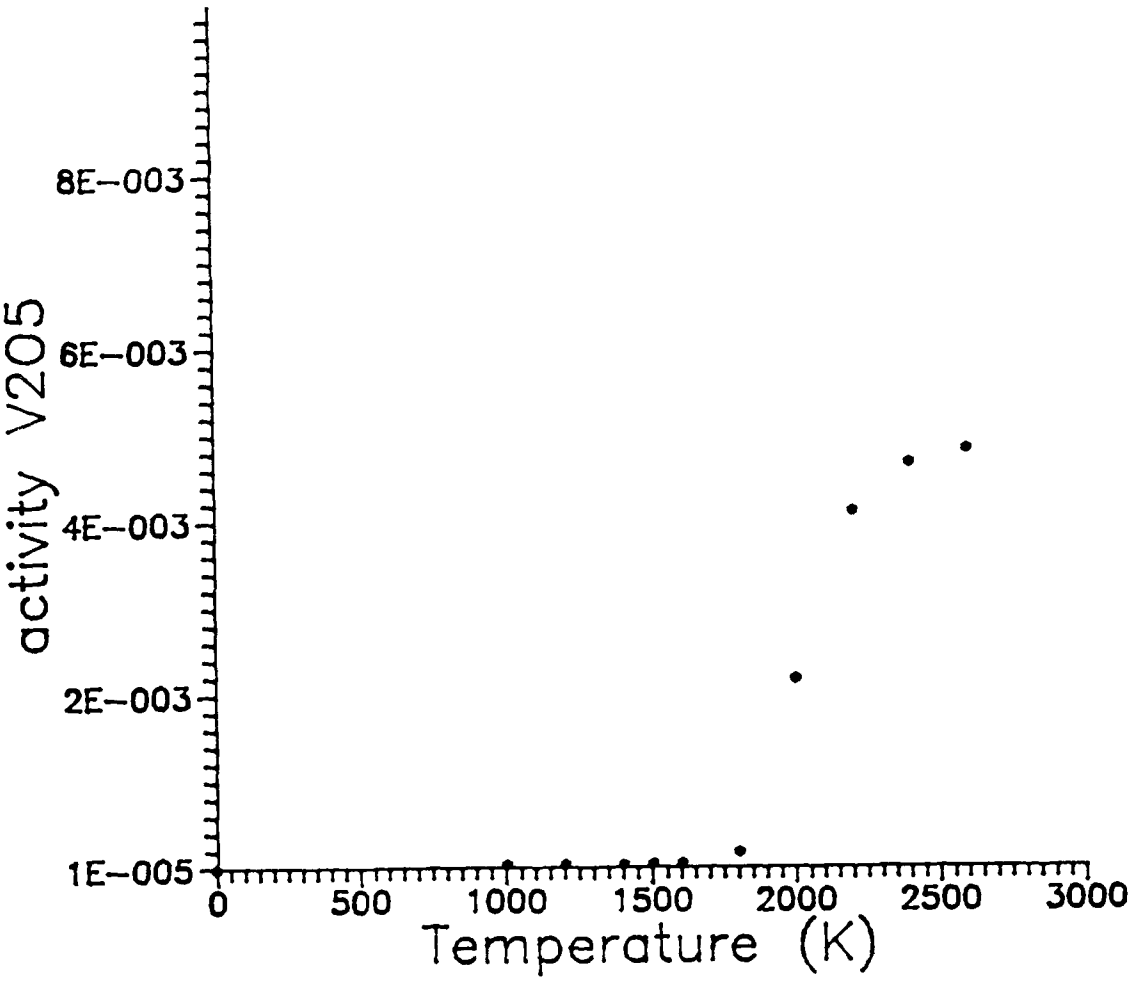

Figure 20. The activity of V_2O_5 versus temperature in a 5 wt% CaO-ZrO_2 at P_{O2} of 10^{-5}

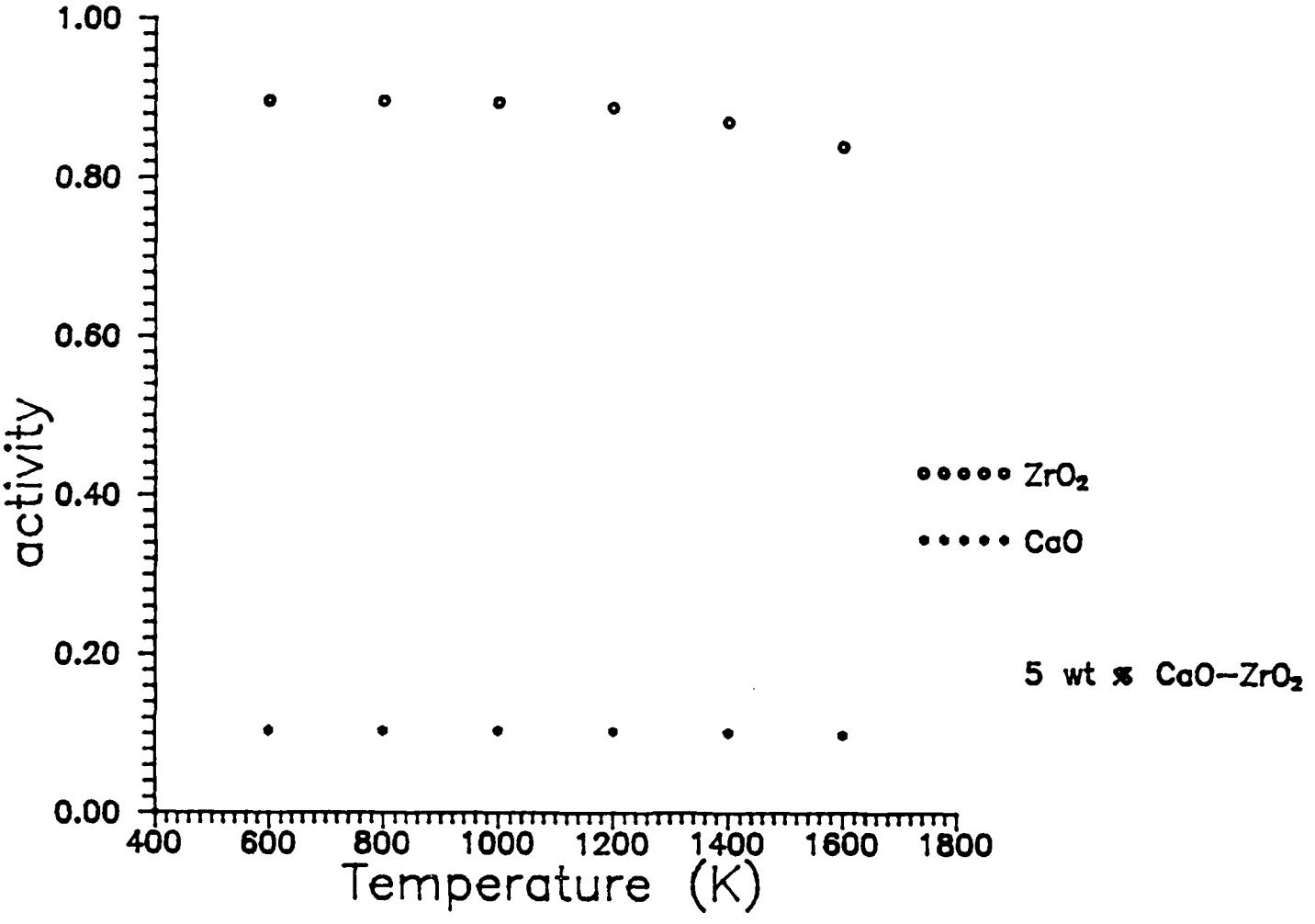

Figure 21. The activities of CaO and ZrO_2 versus temperature in a 5 wt% CaO-ZrO_2 at P_{O2} of 10^{-5}

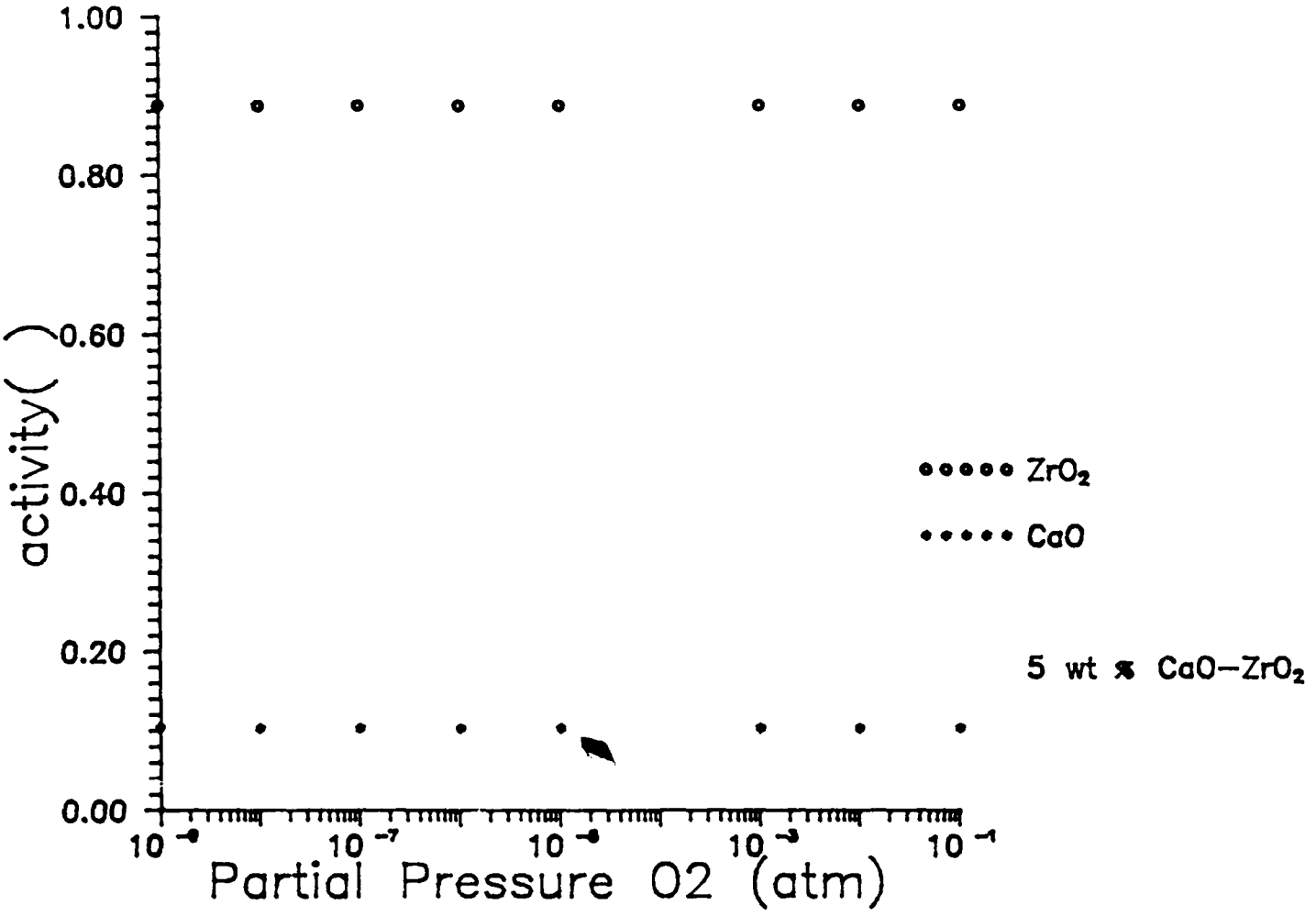

Figure 22. The activities of CaO and ZrO_2 versus P_{O2} in a 5 wt% CaO-ZrO_2 at 1000 K